University of Alberta

Synergy between Erosion and Corrosion of Carbon Steel in Slurry

by

Junfang Lu

A thesis submitted to the Faculty of Graduate Studies and Research in partial fulfillment of the requirements for the degree of Master of Science

in

Materials Engineering

Department of Chemical and Materials Engineering

Edmonton, Alberta, Canada

Spring, 2004

Library and Archives Canada

Published Heritage Branch

395 Wellington Street
Ottawa ON K1A 0N4
Canada

Bibliothèque et Archives Canada

Direction du Patrimoine de l'édition

395, rue Wellington
Ottawa ON K1A 0N4
Canada

Your file Votre référence
ISBN: 0-612-96516-3
Our file Notre référence
ISBN: 0-612-96516-3

The author has granted a non-exclusive license allowing the Library and Archives Canada to reproduce, loan, distribute or sell copies of this thesis in microform, paper or electronic formats.

The author retains ownership of the copyright in this thesis. Neither the thesis nor substantial extracts from it may be printed or otherwise reproduced without the author's permission.

L'auteur a accordé une licence non exclusive permettant à la Bibliothèque et Archives Canada de reproduire, prêter, distribuer ou vendre des copies de cette thèse sous la forme de microfiche/film, de reproduction sur papier ou sur format électronique.

L'auteur conserve la propriété du droit d'auteur qui protège cette thèse. Ni la thèse ni des extraits substantiels de celle-ci ne doivent être imprimés ou aturement reproduits sans son autorisation.

In compliance with the Canadian Privacy Act some supporting forms may have been removed from this thesis.

While these forms may be included in the document page count, their removal does not represent any loss of content from the thesis.

Conformément à la loi canadienne sur la protection de la vie privée, quelques formulaires secondaires ont été enlevés de cette thèse.

Bien que ces formulaires aient inclus dans la pagination, il n'y aura aucun contenu manquant.

Canada

ABSTRACT

Erosion-corrosion is a serious problem in many industrial processes, especially in the oil sands industry because of the processing of silica solids in pipelines. Due to the coexistence of mechanical erosion and electrochemical corrosion, erosion-corrosion is a synergistic damage mechanism. In some conditions, the synergy is a very important wastage component. In order to reduce the erosion-corrosion cost, it is necessary to understand the mechanism.

The synergistic effect between erosion and corrosion of A1045 carbon steel in slurry was investigated. The mechanism of synergy was studied via chemo-mechanical effects under anodic polarization condition. The results indicate that the hardness degradation due to the chemo-mechanical effect is a synergistic mechanism in the slurry-erosion process. However, the values of the synergy estimated from hardness tests are lower than those experimentally determined. Surface analysis revealed that the main mechanism for the synergy is likely pitting corrosion.

ACKNOWLEDGEMENTS

I would like to express my sincerest gratitude and appreciation to my supervisor, Dr. Jingli Luo, for her continuous guidance, support throughout the course of this research. I am impressed by her scientific knowledge, insight and energy. She has provided me with a great deal of inspiration throughout the research.

I would also like to thank Dr. B.T. Lu for ideas and motivation. He has provided me with a great deal of help. His guidance and encouragement has helped me overcome the hardship during this work.

I would like to extend my appreciation to Mr. B. Walter and Mr. E. Vokes for their help that they have provided me. Also I show thanks to Ms. S.L. Lim, Ms. H.X. Guo, Mr. L. Li, Mr. S. Sankaran, Mr. Y. Huang and other group members for their help, their friendship and the contribution towards a good research environment.

My special thanks must be given to my parents, my husband and my lovely son for their love, patience and encouragement during this work. Without them, none of this would have been possible.

TABLE OF CONTENTS

Chapter 1 Introduction 1

1.1 Statement of the problem 1

1.2 Objectives 1

1.3 Outline of the thesis 2

Chapter 2 Literature review 3

2.1 Slurry pipelines and erosion-corrosion 3

2.2 Description of erosion-corrosion 3

2.2.1 General description 3

2.2.2 Classification of erosion-corrosion 4

2.3 Mechanism of erosion and factors controlling erosion 6

2.3.1 Mechanism of erosion and outlines of erosion models 6

2.3.2 Factors controlling erosion 8

2.4 Mechanism of corrosion and factors controlling corrosion 12

2.4.1 Mechanism of corrosion 12

2.4.2 Corrosion in flowing media 14

2.4.3 Factors controlling corrosion 16

2.5 Synergy between erosion and corrosion 19

2.6 Pitting corrosion 22

2.7 Measurement of the erosion-corrosion components 24

2.7.1 Pure corrosive component (w_c) and pure erosive component (w_e) 24

2.7.2 Synergy component (w_s) 25

2.8 Experimental techniques used in erosion-corrosion investigation 26

Chapter 3 Experimental procedures 27

3.1 Test material and heat treatment of specimens 27

3.2 Test solutions 29

3.3 Experimental setup/apparatus 30

3.3.1 Potentiodynamic measurement setup 30

3.3.2 Micro-hardness tester 31

3.3.3 Rotating cylinder electrode (RCE) 32

3.4 Experimental procedures 34
3.4.1 Preparation of the samples 34
3.4.2 Hardness test procedures 34
3.4.3 Erosion-corrosion test procedures 34
Chapter 4 Results and discussions 38
4.1 Hardness degradation due to chemo-mechanical effect 38
4.1.1 Effect of anodic dissolution on surface hardness 38
4.1.2 Chemo-mechanical effect 40
4.2 Microstructure and hardness results after heat treatment 42
4.2.1 Microstructure 42
4.2.2 The relationship between hardness and heat treating temperature 45
4.3 Pure corrosion rate 47
4.3.1 Electrochemical test results--Potentiodynamic polarization 47
4.3.2 Weight loss test results 48
4.4 Pure erosion rate 48
4.4.1 Calibration of the weight loss test 48
4.4.2 Pure erosion rate 50
4.5 Synergy between erosion and corrosion 50
4.5.1 Electrochemical test results 50
4.5.2 Contribution of each wastage component on erosion-corrosion 53
4.6 Mechanism of the synergy 56
4.6.1 Chemo-mechanical effect in erosion-corrosion process 56
4.6.2 Damage of surface morphology due to erosion-corrosion 61
4.6.3 Mechanism of the synergy 72
Chapter 5 Conclusions and future work 73
5.1 Conclusions 73
5.2 Future work 74
Literature Cited 75

LIST OF TABLES

Table 3-1 Chemical compositions of A1045 carbon steel (wt %) 27
Table 3-2 Heat treatment conditions of A1045 carbon steel 28
Table 3-3 Quality parameters of tap water (Source: EPCOR, Edmonton) 29
Table 3-4 Main properties of the silica sand 30

LIST OF FIGURES

Figure 2-1 Interaction of corrosion with erosion associated with liquid flow 4
Figure 2-2 Erosion behaviour of ductile and brittle materials 10
Figure 2-3 Pourbaix diagram for the Fe-H_2O system at 25°C for 10^{-6} M activities of all metal ions 12
Figure 2-4 Schematic diagram showing reactions of carbon steel in neutral solution 13
Figure 2-5 Effect of velocity on corrosion rate 17
Figure 2-6 Effect of oxygen concentration on the corrosion rate of iron in water 18
Figure 2-7 Cathodic protection with an external power supply 24
Figure 3-1 Sample dimension 28
Figure 3-2 Micrograph of silica sand particles 30
Figure 3-3 Corrosion cell used in potentiodynamic measurement 31
Figure 3-4 Schematic illustration of the micro-hardness measurement system 32
Figure 3-5 Schematic illustration of the electrochemical measurement apparatus 33
Figure 3-6 Tafel slope calculation 36
Figure 4-1 Hardness drop vs. anodic current density 38
Figure 4-2 Polarization curves of A1045 in distilled water and 1M $NaHCO_3$ solution 39
Figure 4-3 Schematic lattice structure of surface of a crystal material 41
Figure 4-4 Photomicrograph of A1045 carbon steel under various heat treatment conditions 44
Figure 4-5 Relationship between hardness and heat treating temperature 45
Figure 4-6 Potentiodynamic curves in tap water with various flow rates 47
Figure 4-7 Dependence of the pure corrosion rate on flow rate 48
Figure 4-8 Comparing tests to verify the validity of weight loss test 49
Figure 4-9 Dependence of the pure erosion rate on flow rate and sand concentration 50
Figure 4-10 Potentiodynamic curves in slurry with 20 wt% sand under various flow rates 51
Figure 4-11 Potentiodynamic curves in slurry with 30 wt% sand under various flow rates 51

Figure 4-12 Potentiodynamic curves at 3000 RPM under various sand concentrations .. 52
Figure 4-13 Effect of flow rate and sand concentration on i_{corr} 53
Figure 4-14 Differentiation of each of the wastage component as a function of flow rate in slurry with 20 wt% sand 54
Figure 4-15 Differentiation of each of the wastage component as a function of flow rate in slurry with 30 wt% sand 54
Figure 4-16 Fraction of each wastage component in slurry with 30 wt% sand at 3000 RPM 55
Figure 4-17 Fraction of each wastage component in slurry with 30 wt% sand at 6000 RPM 56
Figure 4-18 Dependence of mechanical erosion rate on hardness in slurry with 20 wt% sand 57
Figure 4-19 Dependence of the normalized synergy rate (w_s/w_e) on the anodic current density in slurry with 20 wt% sand 60
Figure 4-20 Surface morphology of the specimen before erosion-corrosion test 61
Figure 4-21 Surface morphology after static immersion in tap water 62
Figure 4-22 Surface morphology in tap water under open circuit condition 63
Figure 4-23 Surface morphology after static immersion in tap water for 30 minutes under cathodic protection 63
Figure 4-24 XRD result of the deposit—composed by $CaCO_3$ 64
Figure 4-25 Surface morphology in flowing slurry under cathodic protection for 30 minutes at 6000 RPM 65
Figure 4-26 Surface morphology in flowing slurry with 20 wt% sand under open circuit for 30 minutes at 6000 RPM 66
Figure 4-27 Surface morphology in flowing slurry with 20 wt% sand under open circuit for 30 minutes at 6000 RPM 66
Figure 4-28 The SEM micrograph showing deep pit in flowing slurry with 20 wt% sand under open circuit for 30 minutes at 6000 RPM 67
Figure 4-29 Surface morphology after erosion-corrosion for 25 hours in slurry with 20 wt% sand under open circuit at 6000 RPM 67

Figure 4-30 Corrosion pits in slurry with 20 wt% sand, 2.5E-4A/cm^2 anodic polarization for 30 minutes at 6000 RPM 68
Figure 4-31 Comparison of the morphology of wear scars in slurry with 20 wt% sand for 10 minutes at 6000 RPM 69
Figure 4-32 Comparison of the dimensions of wear scars in slurry with 20 wt% sand for 10 minutes at 6000 RPM under cathodic protection and 2.5E-4 A/cm^2 anodic polarization 70
Figure 4-33 Comparison of pit number in different test conditions for 30 minutes 71
Figure 4-34 Area fraction of pits in different test conditions for 30 minutes 71

LIST OF SYMBOLS

Symbols	Meanings
d	Average grain diameter
D	Diffusion coefficient
$E_{applied}$	Applied potential
E_{corr}	Self-corrosion potential
H_D	Dynamic hardness of the target material
H_S	Static hardness of the target material
Hv	Vickers hardness under anodic polarization
Hv_0	Vickers hardness without anodic polarization
i	Measured current density
i_{corr}	Corrosion current density
i_0	Threshold current density
k	Mass transfer coefficient
K_y	Constant for a particular material
mV	Millivolt
N	Mass flux in diffusion controlled process
Re	Reynolds number
Sc	Schmidt number
SEM	Scanning electron microscope
Sh	Sherwood number
TWL	Total weight loss
V	Velocity
w_c	Pure corrosion rate
w_e	Pure erosion rate

w_s	Synergy between erosion and corrosion
β	Tafel slope
β_a	Anodic Tafel slope
β_c	Cathodic Tafel slope
η	Overpotential
v	Kinematic viscosity
σ_0	Constant for a particular material
σ_y	Yield strength
ΔC	Concentration difference of bulk solution/surface
ΔHv	Relative hardness drop
Δw_c	Increment of erosion rate

LIST OF ABBRIVATIONS

Abbreviations	Meanings
AISI	American Iron and Steel Institute
ASTM	American Society for Testing and Materials
CE	Counter electrode
SCE	Saturated calomel electrode
WE	Working electrode

Chapter 1 Introduction

1.1 Statement of the problem

Erosion-corrosion is a serious problem in many industrial processes, such as the oil industry, hydroelectric power plants and mining and piping systems. It can reduce the lifetime at certain components and cause high maintenance costs. In the oil sands industry of Northern Alberta, it is a much more serious problem because of the processing of silica-based solids.[1,2] Therefore, erosion-corrosion has received much more attention in recent years.

Erosion–corrosion in slurry is a synergistic damage mechanism because of the co-existence of mechanical erosion and electrochemical corrosion. Total material loss is normally higher than the sum of the components of the pure mechanical erosion and the pure electrochemical corrosion because of the existence of the synergistic effect.[3,4,5,6] The contribution of synergy to the total material loss is often so important that it cannot be neglected in practical engineering.

The damage caused by erosion-corrosion depends on many variables such as test conditions (i.e. temperature of operation, flow velocity, sand concentration and dissolved oxygen concentration), material properties, particle properties and properties of the corrosion product. Because of the interaction of mechanical and electrochemical factors, the mechanisms of synergistic effects in erosion-corrosion processes are still poorly understood. A clear understanding of the synergy is needed to understand the erosion-corrosion mechanism and to control erosion-corrosion.

1.2 Objectives

An advancing understanding of erosion-corrosion mechanism is a key for developing control strategy of erosion-corrosion. Thus, the present study was undertaken with the following objectives:

(1) To investigate the factors controlling the synergy in slurry-erosion processes.

(2) To understand the synergistic mechanism of the erosion-corrosion.

Each of these components of the research is presented in details in the following chapters of this thesis.

1.3 Outline of the thesis

Chapter 2 covers a review of general erosion and corrosion characteristics. Chapter 3 presents the experimental procedures that were used to meet the objectives of the study. Chapter 4 presents the results and discussions for the hardness test, microstructure, electrochemical test, weight loss test and finally surface morphology analyses. Finally, conclusions are made in Chapter 5 along with the recommendations for the future work.

Chapter 2 Literature review

2.1 Slurry pipelines and erosion-corrosion

Pipeline method is the most economical and well-established method of transporting large quantities of domestic water, oil and other fluids. The transport of mixtures of solids and liquids in pipes is called the slurry pipeline method. Many industries such as chemical, petroleum, metallurgical, pulp and paper, and other industrial plants use this method to transport raw materials, materials in process and finished products in large quantities through their facilities.[7]

The major criterion for comparing the slurry pipeline method to other transportation methods is the economic advantage. It has low cost, high efficiency and high reliability. It is also geographically flexible. It can be used on any terrain and in any processing plant location. They are buried and controlled automatically, and use water as a carrier in most cases; it is very safe and environmentally sound.

Carbon steel pipelines have been widely used for transport in oil sand production in Alberta, where there is a serious erosion-corrosion problem of pipelines. Severe damage has occurred to flow lines, valves, pumps, and other equipment. It costs the petroleum industry hundreds of millions of dollars each year. Therefore, it is very necessary to study the erosion-corrosion mechanism and then to control it.

2.2 Description of erosion-corrosion

2.2.1 General description

The destructive modes which cause degradation of slurry pipelines can be categorized into chemical (or electrochemical) and mechanical. In the former condition, the metal is gradually dissolved by chemical (or electrochemical) process. In the latter condition, material is removed by cracking, rupture and plastic deformation. Erosion is one type of mechanical mode, which is defined as the progressive loss of material from a solid surface due to mechanical interaction between that surface and a fluid, a multi-

component fluid, or impinging liquid or solid particles.[8] So, erosion and corrosion are two different deterioration mechanisms.

When these two modes occur simultaneously, damage will be much higher. The result is owing to the interaction between erosion and corrosion, which is called synergistic effect. Sometimes the synergistic effect is the most important.

2.2.2 Classification of erosion-corrosion

Corrosion can interact with the erosion process under flowing liquid condition. The possible interactions of corrosion and erosion associated with liquid flow are shown in Figure 2-1.[9,10] The area of A, B and C is the conditions for slurry erosion-corrosion, cavitation erosion-corrosion and turbulent flow corrosion, respectively. Both slurry erosion-corrosion and cavitation erosion-corrosion are forms of erosion-corrosion.

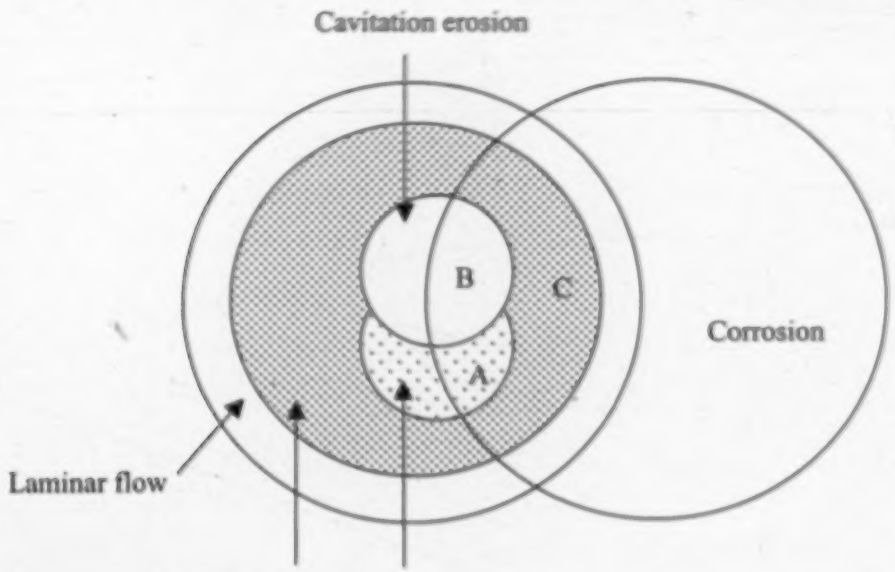

A: Slurry erosion-corrosion

B: Cavitation erosion-corrosion

C: Turbulent flow corrosion

Figure 2-1 Interaction of corrosion with erosion associated with liquid flow[9,10]

(1) Slurry erosion-corrosion

Slurry erosion-corrosion (generally named erosion-corrosion), results from the relative movement between corrosive slurry and the metal surface. The rapid movement of a corrosive liquid over a metal forms grooves, waves or horseshoe-shaped pits, usually in a directional pattern with the open edge of the horseshoes pointing downstream.[11] Erosion-corrosion can be distinguished by its distinctive appearance.

Most metals are susceptible to erosion-corrosion under specific conditions, especially if they rely on a mechanically weak surface film for protection. Carbon steel and low alloy steel, with their weak rust layer, undergo erosion-corrosion.

(2) Cavitation erosion-corrosion

Cavitation erosion-corrosion is caused by the formation and collapse of vapor bubbles in a liquid against a metal surface. The collapse of cavitation bubbles produces high force on the metal surface, which can remove a corrosion product layer and give an active metal surface, leading to damage and material removal. Cavitation occurs in hydraulic turbines, on pump impellers, on ship propellers, and so many surfaces in contact with high-velocity liquids subject to changes in pressure. Cavitation corrosion can be easily distinguished from erosion-corrosion by both phenomenology and mechanism. Cavitation corrosion damage appears as a set of deep, sharp-edged craters on the metal surface.

The causes and mechanisms of cavitation damage are still controversial to some extent. But most authorities agree that there are two main sources of erosion damage.[9] One is the collapse-generated stress wave. When a cavitation bubble collapses, it happens very rapidly and generates a stress wave in the surrounding liquid. The intensity of the stress pulse is higher than the yield stress of many engineering alloys. The other source of erosion damage is the jetting phenomenon. If the bubble is surrounded by a large volume of liquid, it will not collapse with spherical symmetry, it will collapse asymmetrically, forming a jet of liquid directed towards the surface and traveling at high velocity. This jet generates a high impact pressure on striking the surface, which can result in erosion damage.

2.3 Mechanism of erosion and factors controlling erosion

2.3.1 Mechanism of erosion and outlines of erosion models

2.3.1.1 Mechanism of erosion

Micro-cutting mechanism is one of the important erosion mechanisms, which was widely cited from 1958 to about 1975. Finnie[12] developed an important analytical model to predict erosion rate, which is based on the micro-cutting mechanism. It will be explained in the next section.

Now the platelet mechanism is another popular mechanism. It was developed on the basis of the investigation of the work hardening effect and the microscopic sequence observation of erosion.[13] It consists of a sequential plastic deformation process that accounts for each of the separate occurrences that result in the overall surface degradation.[14] The main process of the platelet mechanism is explained as follows. The erosion heated-surface consists of platelets at various stages as the result of plastic strain deformation. Beneath the platelet zone is a work-hardened zone developed during the early stages of the erosion process. Beneath the work-hardened zone is the base metal at its initial condition. The initial platelets are formed without material loss. The platelets are attached to some location along the extrusion path. Beneath the immediate surface region, the mass of target material forms a work-hardened zone. When the surface has been completely converted to platelets and craters and the work-hardened zone has reached its stable hardness and thickness, steady state erosion begins. Because the subsurface work-hardened zone acts as an anvil, the steady-state erosion rate becomes higher. When the platelets are fully formed, the highest material removal rates will occur.[14]

For all of the erosion mechanisms nowadays, the essence of small solid particle erosion is that the surface material is removed by a micro-mechanical deformation /fracture process because of the erosion effect of small, solid, impacting particles on metals. For ductile materials, the impacting particles cause severe and localized plastic

strain to occur that eventually exceeds the strain to failure of the deformed material. For brittle materials, the forces of the erodent particles cause cracking and chipping off of micro-size pieces.

2.3.1.2 Outlines of the erosion models

Nowadays, there are many erosion models used to predict the erosion resistance. The following summarizes the basic principles of the most popular models.

(1) Finnie's model (cutting model)

Finnie's model is a cutting model of ductile metals.[15] This model was based on the premise that individual erodent particles traveled along the surface of the target metal. The volume of material removed was calculated from the trajectory of each particle and the amount of cutting that would occur as the result of pure plastic deformation with no cracks propagating ahead of the eroding particle.

At low grazing angles, the idealized particle strikes the surface, forms a crater and then leaves the surface. Observations with stereo scanning electron microscopy showed that some particles remove a chip as in metal cutting, others leave material piled up at the sides or the end of the crater. The raised material is presumably removed relatively easily by subsequent particles.[16] Finnie's model is good for ductile specimens at small angles of attack; however it makes no predictions for the erosion which occurs under normal attack on such materials.

(2) Bitter's model

Bitter[17,18] proposed that the erosion of ductile metals comprises two mechanisms occurring simultaneously. One is caused by repeated deformation during collisions, eventually resulting in detachment of materials; the other is caused by the cutting action of the free moving particles. Deformation wear occurs when the particles kinetic energy to cause local stresses is higher than the yield strength of the pipe. Cutting wear occurs when the particles have sufficient energy to shear the local surface. In addition, Bitter allows for deformation wear which is associated with the repeated blows suffered by the

specimen and which eventually cause cracking and spalling of surface material. It is this deformation wear that accounts for the erosion at normal attack in ductile materials and which is not accounted for in Finnie's analysis.

(3) Hutchings' model (fatigue model)

Hutchings[19] uses the concept of low cycle fatigue to describe erosion at normal impact and thus the model is known as the 'fatigue' model. This theory proposed that since erosion involves the accumulation of plastic deformation in the surface layers of the material, the maximum plastic strain within a fragment of material must be attained before detachment of material in the form of platelets can occur. This maximum strain term was termed the critical strain.

(4) Sundararajan's model

Sundararajan's first model is named 'localized model',[20] which is similar to Hutchings' fatigue model. It employed a critical strain criterion to explain solid particle erosion at normal impact by assuming that the formation of a localized lip of material along the rim of the crater and its removal during subsequent impacts were mainly responsible for material loss at 90°. The formation of the localized lip occurred once a critical strain was exceeded in the deforming volume beneath the impacting particle. Sundararajan's second model[21] was a model for solid particle erosion for all impact angles and any shape of eroding particle. This model was split into two components. One expression was for erosion at normal impact based on the volume of localized plastic deformation beneath the impacting particle. The other was for small impact angles based on the energy absorbed in shear.

2.3.2 Factors controlling erosion

There are many factors that can affect erosion, such as flowing parameters, slurry properties and target material properties. For flowing parameters, it includes flowing regimes, flowing velocity, and impact angle. For slurry properties, they include particle properties (such as particle concentration, composition, hardness, shape, particle size and

particle degradation) and liquid properties. Metal properties include surface topography, residual stress level, hardness, ductility and microstructure of the materials.

2.3.2.1 Flowing parameters

(1) Flowing velocity

Erosion is strongly dependent on slurry velocity. Flow rate can enhance the erosion action on the metal surface by removing passive layers, producing a more reactive surface. Most published work shows that power law dependence is followed. The erosion rate is proportional to the velocity raised to some exponent. The value of the velocity exponent varies in the range from 1 to 4. Values of about 3 are often found.[9] The increase in erosion with flowing rate is assumed to be due to the increase in kinetic energy of the solid particles whose impact energy increases as the square of the velocity.[22]

(2) Impact angle

There are two different modes of erosion response of a material: ductile and brittle. The main difference between these two modes is the manner in which the erosion rate varies with the angle of impact. The erosion rate versus angle of impingement for ductile and brittle materials is shown in Figure 2-2.[23]

For ductile materials, maximum erosion occurs at low angles, usually found to be 15° to 30°. Most metals and alloys exhibit this behavior. Most of the investigators believe that the failure is mainly due to extensive plastic deformation of surface material. Brittle materials behave quite differently than ductile materials. For brittle materials maximum erosion occurs at normal impact. Most ceramics and glasses exhibit this behavior. The failure is mainly related to crack propagation and chipping.

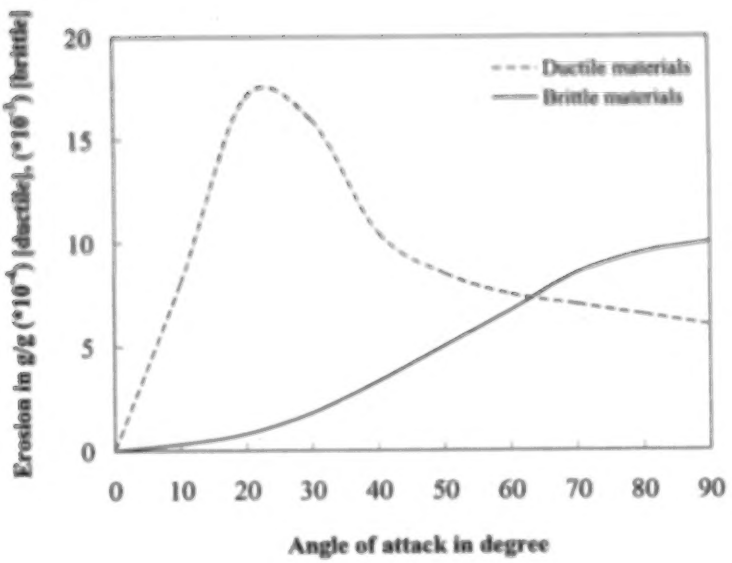

Figure 2-2 Erosion behaviour of ductile and brittle materials[23]

2.3.2.2 Particle properties

(1) Particle concentration

Slurry erosion rates increase with increasing particle concentration.[22,24,25,26] The effect decreases with increasing particle concentration due to particle-particle interaction.[22,24,26]

(2) Particle hardness

Particle hardness has a strong influence on slurry erosion. It is found that if the hardness of a particle is greater than about 1.2 times that of the target material, the particle can scratch the surface, causing a much higher wear rate. If the hardness of the particle is lower than about 1.2 times, scratching does not occur; the erosion rate will be much lower. If the hardness of particles is significantly greater than the surface, the increase will not cause a significant effect on the erosion rate.[9]

(3) Particle shape

Particle shape is a major factor in erosion. In order to determine the effect of particle shape on erosion rate, identically sized steel particles in both angular and spherical shapes were used to erode AISI 1020 steel.[27] The angular steel grit caused much sharper, deeper craters to form more platelets, while the spherical steel caused fewer platelets. This showed that angular particles can concentrate local force more efficiently than rounded particles. The more sharp and angular the particles are, the higher the erosion rate will be.

(4) Particle size

There is a peak mass loss that occurs at a certain particle size. Below this size, the kinetic energy of the particles is too low to remove target materials effectively. At particles sizes greater than this size, the particle's ability to penetrate the target surface is reduced. With the larger diameter and more mass of the particles, the effective removal of materials to cause severe plastic deformation formed by platelet is reduced.[27]

(5) Particle degradation

Particles suffer successive degradation because of their continuous contact with the containing wall as they flow through pipes or pumps. Particle size can be reduced by fracture or particle shape can be rounded. The abrasivity of the particles is reduced and, therefore, the erosion rate will be reduced. For a small slurry rig, particle degradation is large because of the small volume of slurry used. Large pipe loop systems do not have very serious particle degradation because of the large volume of slurry used.

2.3.2.3 Mechanical properties of target materials

Hardness of the materials is a fairly good criterion for predicting resistance to straight erosion. In Finnie's model,[15] the erosion rate is inversely proportional to the static hardness (H_s) of the target material. In Bitter's and Sundararajan's model,[18,20] the erosion rate is inversely proportional to the power of the static hardness (H_s) of the target material. In Hutchings' model, the erosion rate is inversely proportional to the

power of the dynamic hardness (H_D) of the target material. In general, soft metals are more susceptible to mechanical erosion than hard metals. The harder the matrix, the more erosion resistant it is.[28] It was also confirmed that increasing the hardness of steel was effective in improving erosion resistance in a slurry environment.[3,29]

2.4 Mechanism of corrosion and factors controlling corrosion

2.4.1 Mechanism of corrosion

Corrosion is an electrochemical phenomenon that requires an anode, a cathode, an ion conduction path--an electrolyte solution and an electrical connection for electrons flow between anode and cathode. The potential-pH diagram (Pourbaix diagram) for the Fe-H_2O is shown in Figure 2-3.[30]

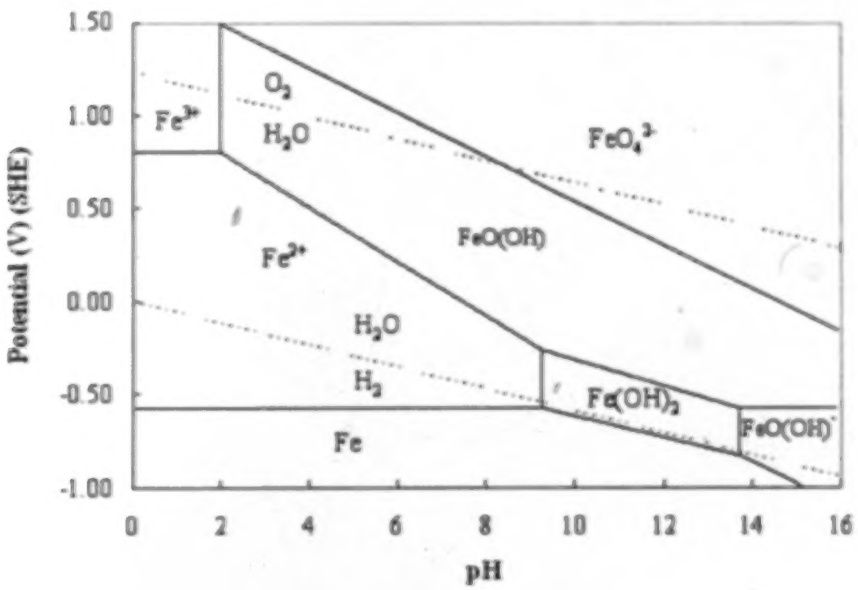

Figure 2-3 Pourbaix diagram for the Fe-H_2O system at 25°C for 10^{-6} M activities of all metal ions[30]

From the Pourbaix diagram, the anodic and cathodic reactions for steel in neutral or basic solutions containing dissolved O_2 are shown as follows. The schematic illustration of the reaction of steel at the interface of the steel and solution is shown in Figure 2-4.

$$2Fe \longrightarrow 2Fe^{2+} + 4e^- \quad \text{(the anodic reaction)} \qquad (2\text{-}1)$$

$$O_2 + 2H_2O + 4e^- \longrightarrow 4OH^- \quad \text{(the cathodic reaction)} \qquad (2\text{-}2)$$

The total cell reaction is

$$2Fe + O_2 + 2H_2O \longrightarrow 2Fe^{2+} + 4OH^- \longrightarrow 2Fe(OH)_2 \qquad (2\text{-}3)$$

$$2Fe(OH)_2 + 1/2O_2 + H_2O \longrightarrow 2Fe(OH)_3 \qquad (2\text{-}4)$$

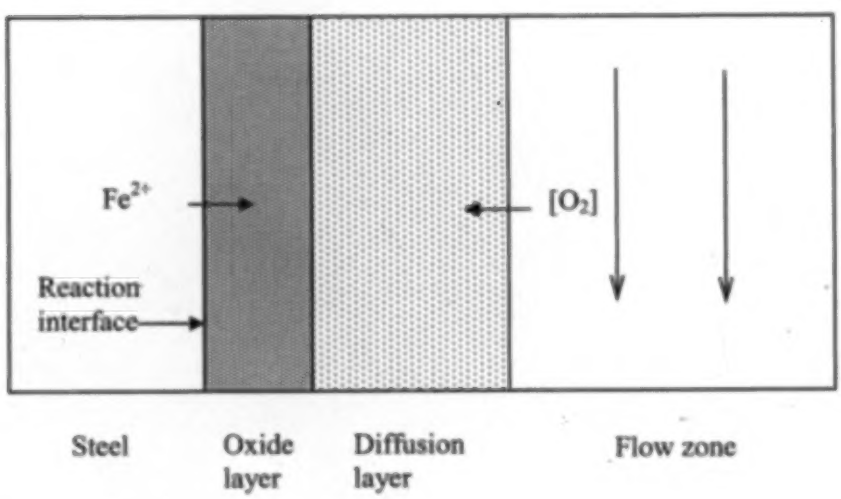

Figure 2-4 Schematic diagram showing reactions of carbon steel in neutral solution

From a physical-chemical point of view, corrosion reactions are heterogeneous reactions. The corrosion of metals and alloys involves at least three fundamental steps: (1) Transport of the reactant to the metal surface. (2) Electron exchange resulting in metal loss. (3) Transport of the corrosion products from the surface to the solution. The corrosion processes are controlled by the slowest step. The corrosion process can also be explained in Figure 2-4. The cathodic reactant--O_2 diffuses from the bulk solution to the metal surface, where electrons are exchanged. Then the corrosion product is transported away from the metal surface to the solution.

2.4.2 Corrosion in flowing media

Some researchers indicate that the corrosion in flowing media is controlled by the mass transfer process. Mass transfer means that ions and molecules reach the metal surface by diffusion as a result of a concentration gradient and chemical activity. For the mass transfer-controlled corrosion, the corrosion rate is affected by either the transport of corrosive species to the metal surface or the dissolved corrosion products away from the surface.

Mass transfer is inherently correlated with liquid flow.[31] The reaction rate in a stagnant solution is very small because the concentration gradient is small (or the thickness of the diffusion layer is big). But if the reactants are transported by convection (due to laminar or turbulent flow), the amount of matter reaching the surface is greatly increased and the reaction rate rises greatly. This kind of transport is known as convective diffusion, which consists of convection in the bulk of solution and diffusion in the immediate vicinity of the surface. The total flux is equal to the sum of diffusion mass transport and convective mass transport.

In the case of oxygen corrosion inside a pipe, a model of flow-dependent corrosion under mixed control is derived.[11,32] It assumes the oxygen transport and electrochemical reaction to be rate-determining and consists of the following steps, as shown in Figure 2-4. (1) Transport of oxygen from the bulk of the flowing aqueous medium to the surface of the solid. (2) Diffusion of the oxygen in the pores of the surface

layer formed by corrosion products on the metal surface. (3) Electrochemical phase boundary reaction of the oxygen with the metal surface at the bottom of the pores.

Various hydrodynamic parameters have been suggested as controlling the occurrence and extent of flow assisted corrosion. For turbulent flows, the mass transport correlation can be expressed as

$$Sh = aSc^{b}\,\mathrm{Re}^{c} \tag{2-5}$$

This equation contains the following dimensionless groups:

- Sherwood number (Sh): Ratio of total mass transport to mass transport by molecular diffusion.

$$Sh = \frac{Kd}{D} \tag{2-6}$$

- Schmidt number (Sc): Ratio of momentum transport to mass transport by molecular diffusion.

$$Sc = \frac{\nu}{D} \tag{2-7}$$

- Reynolds number (Re): Ratio of inertia force to friction force.

$$\mathrm{Re} = \frac{Vd}{\nu} \tag{2-8}$$

Where K is the mass transfer coefficient ($m.s^{-1}$);

d is the characteristic dimension (m);

D is the diffusion coefficient ($m^2.s^{-1}$);

ν is the kinematic viscosity ($m^2.s^{-1}$);

V is the fluid velocity (m/s);

a, b, c are constants. b is typically 0.33, c is between 0.5 and 1.

The mass transfer coefficient K is the parameter relating the rate (N) of a diffusion-controlled reaction to the concentration driving force (ΔC). It incorporates both diffusion and turbulent transport process:

$$N = k\Delta C \tag{2-9}$$

Where N is the mass flux ($mol.m^{-2}.s^{-1}$);

K is the mass transfer coefficient ($m.s^{-1}$);

ΔC is the concentration difference between bulk solution and surface ($mol.m^{-3}$).

This mass transfer correlation has significant uses because Sh can be converted into corrosion rate w via the mass transfer coefficient K, and Re is a function of flow rate V. So the flow dependency of corrosion rate w can be expressed as

$$w = const.V^c \tag{2-10}$$

The equations for mass transfer-controlled corrosion are valid only for mass transfer as the rate-determining step. If additionally electrochemical or chemical steps influence the overall rate, the mixed-control case comes out. The relationship between corrosion and flow rates can no longer be expressed by a simple law because the corrosion reactions through mixed control are less sensitive to changes of flow rate.

2.4.3 Factors controlling corrosion

2.4.3.1 Fluid velocity

Velocity influences the mechanism of the corrosion reaction. The relative velocity between metal and environment can profoundly affect the corrosion rate.

For diffusion-controlled corrosion process, the corrosion rate is enhanced by flowing liquid, shown in Figure 2-5 (a).[30] There are two main reasons. First, flowing liquid removes corrosion products. Second, increasing velocity may increase the supply

of reactant (usually O_2) to the electrode surface because the diffusion of the reactant is often the rate-controlling step, until the velocity gets so high that diffusion is no longer rate controlling. In this case, the corrosion rate is independent of the fluid velocity.

For metals that can passivate, increasing velocity could increase corrosion until a passive film forms. Then velocity has virtually no effect until the velocity becomes so great that it sweeps off passive film from the surface and the corrosion rate is increased. This situation is illustrated in Figure 2-5 (b).[30]

For metals that are protected by a thick layer corrosion product, at low velocity, the corrosion rate almost has no change. But at a critical velocity, corrosion rate increases greatly because that the protective layer is eroded away, shown in Figure 2-5 (c).[30]

For the rather uncommon corrosion process under active controlled, the velocity of the solution has no effect on corrosion.

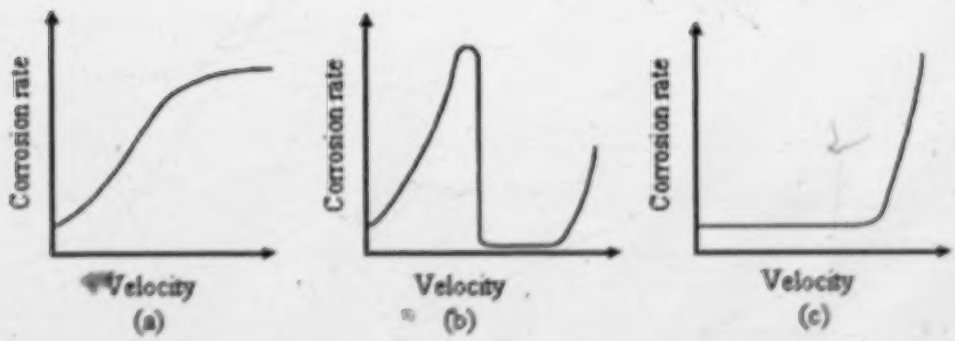

Figure 2-5 Effect of velocity on corrosion rate[30]

(a) Diffusion-controlled corrosion of an active metal with soluble corrosion products.

(b) Active-passive metal.

(c) Metal protected by a thick scale of corrosion product.

2.4.3.2 Dissolved oxygen concentration

Oxygen can influence erosion-corrosion in three ways. Oxygen can control the corrosion rate, corrosion potential and be present as gas bubbles.

In neutral or alkaline solutions, the corrosion rate of steel may be controlled by the cathodic oxygen reduction reaction. Therefore, increasing the concentration of dissolved oxygen increases the corrosion rate, shown in Figure 2-6.[33] This is why severe limitations are usually placed on the oxygen concentration in feed water to steam generation equipment in thermal power stations.[34] Figure 2-6 also shows that the corrosion rate of iron increases with increasing temperature at any given oxygen concentration.

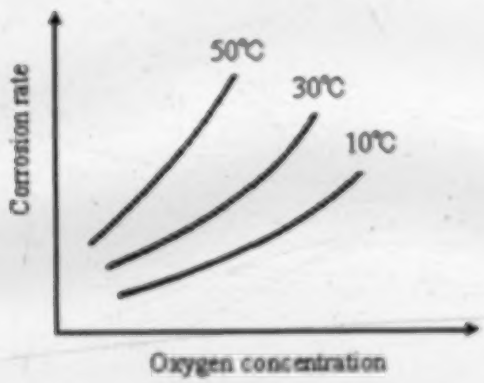

Figure 2-6 Effect of oxygen concentration on the corrosion rate of iron in water[33]

E_{corr} is a function of oxygen concentration. Increasing the dissolved oxygen concentration can increase the availability of the oxygen at the interface, which will shift the free corrosion potential E_{corr} in a positive direction.[35] If the concentration of dissolved oxygen is reduced, the rate of the cathodic reaction will be decreased. Therefore, the overall corrosion rate is decreased. Oxygen can also be present in an undissolved state as gas bubbles adsorbed on particles.[36] Increasing bubble size increases the turbulence, therefore, the severity of impingement attack increases due to cavitation damage.[37]

2.4.3.3 Operation temperature

Increasing temperature increases reaction rates, diffusion rates of reactants and corrosion products for active and passivated metals.

For active reactions, the process of the anodic reaction will be accelerated with an increase of the solution temperature. Therefore, the dissolution rate of the metal is accelerated. But in an aerated solution, the concentration of oxygen is decreased with increasing temperature. Therefore, the cathodic reaction is decreased. Combining these two factors, in general, the dissolution rate of the metal is accelerated.[30]

For passivated metals, as the temperature increases, the protective film breaks down and repairs itself much more rapidly. It becomes more easily damaged by Cl^- ions and thus more susceptible to pitting. At some point the film breaks down entirely and the metal becomes transpassive, corroding at a very high rate.[30]

2.5 Synergy between erosion and corrosion

From the above analyses, the erosion resistance of materials depends mainly on materials' mechanical properties, slurry properties, and the test conditions—hydrodynamic parameters. The corrosion resistance is governed by the chemical characteristics of the material and the test conditions--temperature and environmental corrosivity.

Both theoretical analysis and experimental results have indicated that the mechanical erosion resistance increases with rising strength or hardness[3,29] and the dependence of erosion resistance on the strength/hardness relies on the composition and microstructure of materials.[24,38,39] Relationships have also been established between the corrosion rate and the fluid dynamic parameters under the condition that corrosion is controlled by the mass transport process. However, the erosion-corrosion problem is more complicated because erosion and corrosion interact resulting in the synergistic effect. This means that the mechanical and chemical factors interact with each other.[40,41,42] The interaction of erosion and corrosion could occur in two ways. One is that

the mechanical erosion can result in an increase in the corrosion rate. Second is that corrosion increases the erosion rate.

There are many synergistic mechanisms between erosion and corrosion proposed by researchers. They all believe that erosion and corrosion interact, which causes much greater damage to the material.

Postlethwaite[43,44] believes that mechanical erosion can prevent the formation of a complete rust film for steel; therefore, bare metal is exposed to be rapidly attacked. Erosion can also enhance the convective mass transfer at the metal-fluid interface by solid particles disrupting the diffusion boundary layer; therefore, oxygen diffusion to the corroding surface is enhanced.[44,45] Postlethwaite[46] also proposed that corrosion can roughen the metal surface, which in turn increases the erosion rate because erosion is very sensitive to the impact angle of the solid particles.

R.J.K. Wood[10,47] believes that corrosion can remove work hardened surfaces, exposing the underlying softer base metal to erosion. He also believes that corrosion can cause preferential corrosive attack at grain boundaries resulting in grain loosening and eventual removal. Some other researchers[48,49,50] proposed that the new surface has higher corrosive activity[51]because of the formation of "strain difference cell" by erosion.

It has been found that no simple relationship exists between the erosion-corrosion resistance and hardness.[3,52] This may be because of the existence of synergy. The interaction of many parameters in erosion-corrosion makes the synergistic effect so complicated that the mechanism for synergy of erosion-corrosion is, as yet, poorly understood.[53,54] But synergy is really an important component in practical erosion-corrosion processes that it can never be neglected.[55, 56] Madsen[24,57] reported that 23% to 33% of the total weight loss of low alloy steels could be attributed to the synergistic effect and that this effect increased to 55% to 62% for 18-8 austenitic stainless steels. A. Neville[3] found that the synergistic effect can contribute to 17%-30.4% for different low alloy steel and stainless steels in a slurry condition. Yue et al.[58] found that, when the chrome white iron was eroded in low pH slurry, the contribution of synergy could be as high as 86.3%.

There is still no theory to explain the synergy in a quantitative way. Neville et al.[41] pointed out that the preferential dissolution of a matrix in a flowing corrosive

medium made the hard particles in the microstructure more easily removed, and then erosion will be accelerated because the material loses its erosion resistance. However, this assumption can only offer a qualitative explanation for the accelerated erosion by corrosion in materials with multiphase structures and cannot explain that of single phase materials, such as austenitic stainless steels.

Some Russian researchers[59,60] found that the mobility of dislocations increases with the increase of anodic dissolution current density and then the surface hardness and flow stress of materials decrease. For example, when the passive-to-active condition transition occurs, the hardness of austenitic stainless steels decreases 30-50%, while the anodic dissolution current density increases 50 to 100 times. This phenomenon is defined as a chemo-mechanical effect.[59,60]

Chemo-mechanical behavior is a phenomenon that the physical-mechanical properties changes by chemical (electrochemical) reactions. Chemo-mechanical behavior includes such important phenomena as chemo-mechanical polishing, stress corrosion cracking, corrosion fatigue, erosion-corrosion, etc. It has been found that the mechanical strength of metals will decrease with simultaneous anodic dissolution because of the chemo-mechanical effect,[59,60] and it indicates that the wear resistance of materials will decrease with the presence of corrosion, since the wear-resistance of metals normally increases with increasing hardness. In light of this principle, a chemo-mechanical polish (CMP) process has been developed for grinding hard materials.[61] Obviously, the chemo-mechanical effect is one of the potential mechanisms of the synergy because corrosion current is generated during the erosion-corrosion process in pipelines used to transport slurry in oil sands production. Unfortunately, the concept of corrosion-induced hardness/strength degradation has not yet been applied in the synergism mechanism study under slurry-erosion conditions, which will be studied in the present thesis.

Many researchers[2,49,62,63,64,65] in their erosion-corrosion studies found that pitting corrosion occur on the specimen surfaces. Therefore, pitting is probably one of the synergistic effects, which will also be studied in this research.

2.6 Pitting corrosion

Pitting is one kind of localized corrosion that results in relatively rapid penetration at small areas. Because pits are often very small at the surface and they are easily hidden by corrosion products, they cause much more unexpected damage than other forms of corrosion.

Generally speaking, there are two different stages in the development of pitting corrosion: initiation and propagation. For the first stage, pitting initiates as a localized breakdown of a protective film at weak spots in the film, such as scratches or inclusions on the metal.[30] Normally, breakdown is followed by rapid film repair. If the damaging conditions persist long enough, the film can not repair itself and a pit is initiated. Once initiated, the pit prevents easy mass transport between the pit interior and the exterior solution. But anodic and cathodic reactions have been created inside the pit. Copious anodic production Fe^{2+} attracts negatively anions such as Cl^- to the initiation site to form $FeCl_2$, which will react with water by the reaction

$$FeCl_2 + 2H_2O \longrightarrow Fe(OH)_2 + 2HCl \qquad (2\text{-}11)$$

Hydrochloric acid lowers the local pH at the initiation site. It also releases the Cl^- ion to react with more Fe^{2+}. The acid chloride solution breaks down the passive film, further accelerating anodic dissolution. Pitting corrosion is a serious problem for many stainless steels.

Many researchers studied pitting corrosion with different materials under different conditions. H.M. Shalaby[66] studied the corrosion behavior of high-silicon cast iron in flowing seawater. Pitting attack was found in the regions rich in carbon. Z. Xia and K.C. Chou[67] investigated the susceptibility of carbon steel (pipeline steel) to pitting at room temperature in a deaerated sodium chloride solution saturated in carbon dioxide. They found that pitting resulted from the action of galvanic couples between different sites on the steel surface, either uncovered or screened by porous layers of various corrosion products.

Some researchers investigated pitting corrosion in erosion-corrosion conditions. It is believed that a combination of erosion and corrosion can lead to extremely high pitting rates due to the relative motion of a corrosive fluid next to the metal surface.[68] The increased turbulence caused by pitting on the surfaces can result in rapidly increasing erosion rates.

G. T. Burstein and K. Sasaki[69] studied the corrosion pits of 304L stainless steel in aqueous chloride silica slurry. They found that the metastable pit events after particle impingement are more numerous than those under non-erosive conditions. This means that the erosive impact by solid particles stimulates pitting corrosion. They also found that the metastable pits are born preferentially at the particle impact surface; therefore, they proposed that the synergism in slurry erosion-corrosion arises from the erosive particle impact. The impact of erosive particles causes rupture or removal of the passive film on the surface, exposing fresh active sites during erosion, and therefore pitting corrosion is enhanced.

Uchida, T [70]studied the influence of suspended solids on pitting of carbon steel in cooling water. He found that pit number and pitting depth increased with addition of suspended solids. However, less pits occurred without suspended solids.

R. J. Noel and A. Ball[49] found serious pitting corrosion of mild steel in their synergistic studies of abrasion and corrosion. Before the corrosion test, the mild steel specimens were lightly abraded. Therefore, a wear track was made by abrasion. On both sides of the isolated wear track are ridges that are plastically deformed, containing a high density of dislocations, which present a high internal energy. If the abraded surface is in contact with an electrolyte, a galvanic cell is set up with the ridges acting as the anode. This corrosive attack takes the form of deep multiple pitting along the deformed ridges.

From the above analyses, pitting corrosion is one of the prevailing forms of deterioration of engineering metals. It can be initiated by a number of causes, such as external stress (i.e. impact of solid particles), scratches, microstructure difference and scale, etc. Therefore, the occurrence of pitting corrosion in the erosion-corrosion process is easily understood because of the impact of solid particles. If the target material has multi-phase microstructures, it is also helpful to initiate pitting.

2.7 Measurement of the erosion-corrosion components

2.7.1 Pure corrosive component (w_c) and pure erosive component (w_e)

The pure corrosive component w_c is defined as the corrosion rate free of erosion, induced only by the flowing corrosive medium. It can be evaluated by the weight loss of samples in tap water.

The pure erosive component w_e is defined as the erosion rate free of corrosion. It is measured under the conditions where the corrosion is suppressed. In order to isolate the erosion component of material loss, the specimen is exposed under cathodic protection (CP) during the tests. It is achieved by applying an electric current from a separate power source, shown in Figure 2-7.

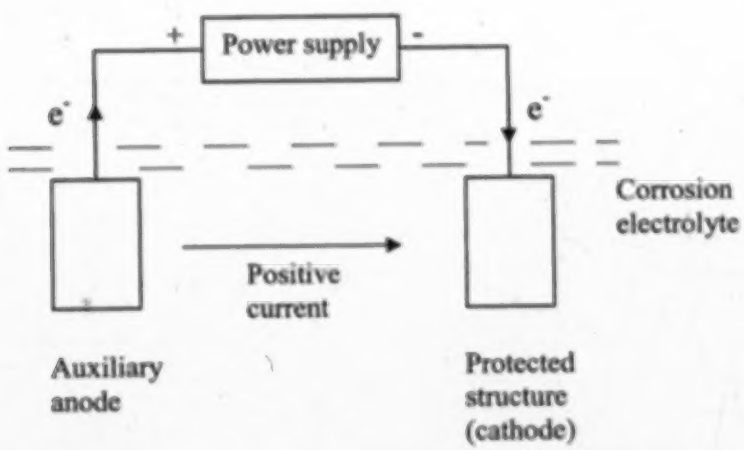

Figure 2-7 Cathodic protection with an external power supply

Cathodic overprotection can cause hydrogen embrittlement—the loss or reduction of ductility of a metal alloy (often steel) as a result of the diffusion of atomic hydrogen into the material. From Figure 2-3 (Pourbaix diagram for the Fe-H_2O system), under a cathodic overprotected condition, the reduction reaction is no longer the reaction of oxygen only. The reduction reaction involves both oxygen and hydrogen. Lots of

hydrogen atoms form on the surface of the metal. Then they diffuse from the surface into the metal phases. By a catalytic effect of some inclusions, these hydrogen atoms are reunited into hydrogen molecules and accumulate in the vacancies inside the metal, reaching very high pressure. The pressure of hydrogen may reach to several hundreds of atmospheres. When hydrogen accumulates for a long time, mechanical properties of the metal will be decreased. The level of CP was chosen to avoid hydrogen evolution at the specimen surface, but negative enough to reduce the corrosion to an insignificant level.

2.7.2 Synergy component (w_s)

Because of the synergistic effect, total material loss rate is normally higher than the sum of components of the pure mechanical erosion free of corrosion (w_e) and the pure electrochemical corrosion free of erosion (w_c).[3, 4, 5]

$$TWL = w_e + w_c + w_s \tag{2-12}$$

Where

TWL is the total weight loss rate induced by erosion, corrosion and synergy.

w_e is the pure erosion rate, free of corrosion.

w_c is the pure corrosion rate, free of erosion, induced only by the flowing corrosive media.

w_s is the synergy between erosion and corrosion.

When w_c and w_e are deducted from TWL, synergy component w_s between erosion and corrosion is obtained.

2.8 Experimental techniques used in erosion-corrosion investigation

There are many techniques used to study the erosion-corrosion behavior of materials such as flow through pipes, nozzles, orifices; impinging jet; rotating disk and rotating cylinder.

Flow through pipes, nozzles and orifices is very useful for examining the influence of actual models of plant conditions.

In the impingement jet technique, the flow characteristics have been very well defined, so precise study of the influence of flow variables on the erosion-corrosion damage can be made.

In the rotating disc technique, a disk is rotated at a fixed angular velocity. This technique can study a range of liquid velocities at the same time. The liquid velocity increases from zero at the axis of rotation to a maximum at the disk periphery.

In the rotating cylinder (RCE) technique, a cylinder is rotated about its axis of symmetry. The surface of the cylinder provides a curved surface exposed at a constant velocity to the solution if the rotational velocity is controlled. Compared with other erosion-corrosion apparatus, this system has many advantages. It is easy to construct. The erosion-corrosion is uniform over a relatively large surface area, and the electrochemical measurement can be easily arranged so that the corrosion and erosion rate can be separated. This technique was used in present research.

Chapter 3 Experimental procedures

Six types of tests were conducted in this research. (1) Hardness test under anodic polarization condition to study the chemo-mechanical effect. (2) Potentiodynamic scans to determine the corrosion current density. (3) Weight loss test to determine the total erosion-corrosion rate and pure corrosion rate. (4) Weight loss test under cathodic protection to determine the pure erosion rate. (5) Anodic polarization method to study the relationship between the synergy and corrosion current density. (6) Surface morphology analysis by optical microscope and SEM to reveal the synergy mechanism.

The synergy between erosion and corrosion was determined by separating the pure erosive and corrosive component and comparing them with the total erosion-corrosion rate. The test parameters were solid concentration and rotating speed of the test specimen.

3.1 Test material and heat treatment of specimens

AISI 1045 (or A1045) carbon steel rod with a diameter of 25.4 mm was used as the test material. In the as received condition, it has typical pearlite and ferrite microstructure. The chemical compositions are listed in Table 3-1.

Table 3-1 Chemical compositions of A1045 carbon steel (wt %)

Steel	C	Mn	S	P
A1045	0.43-0.50	0.60-0.90	0.05max	0.04max

In the hardness test, the as-received material was used. In the erosion-corrosion test, all of the specimens were cylindrical. The specimens were machined and ground to the desired dimensions as shown in Figure 3-1.

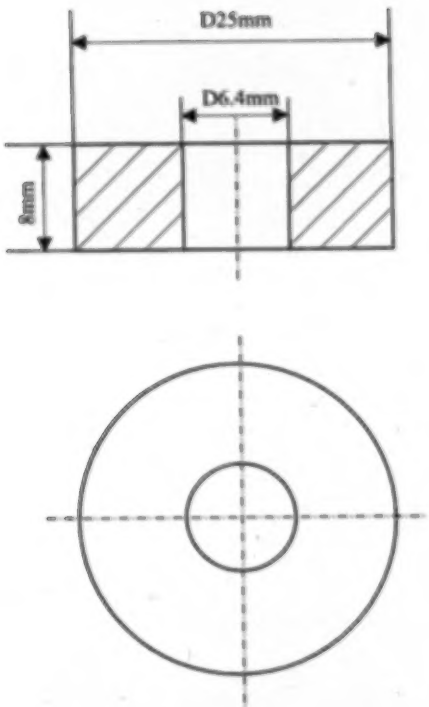

Figure 3-1 Sample dimension

In order to investigate the effect of hardness on the erosion-corrosion process, the machined samples were put into a quartz tube, annealed or tempered in the furnace for 1 hour at different temperatures to vary the hardness. During the annealing or tempering process, nitrogen was used to protect the specimens from oxidation. The heat treatment is shown in Table 3-2.

Table 3-2 Heat treatment conditions of A1045 carbon steel

Treated condition	Processing conditions
Hot extruded	As-received condition
Tempered	500 ℃ for 1h/Furnace cooling
Annealed	850 ℃ for 1h/Furnace cooling
Annealed	1050 ℃ for 1h/Furnace cooling

Microstructures of the specimens were analyzed by an optical microscope after the samples were etched by 2% nital for 15-20 seconds. After heat treatment, specimens with different hardness were obtained. Erosion-corrosion tests were conducted with these specimens under cathodic protection conditions.

3.2 Test solutions

Distilled water and $NaHCO_3$ are two typical systems used for investigating erosion-corrosion behaviour. Steel has different dissolution behaviours in these two solutions. In order to understand the effect of chemo-mechanical effect under different corrosion conditions, distilled water and 1M $NaHCO_3$ were used in hardness test.

The erosion–corrosion tests were conducted in the slurry of silica sand + tap water with different sand concentration. The quality parameters of EPCOR's treated water are shown in Table 3-3.[71]

Table 3-3 Quality parameters of tap water (Source: EPCOR, Edmonton)

Ions	Fe^{2+} (mg/L)	Mg^{2+} (mg/L)	Na^{+} (mg/L)	K^{+} (mg/L)	Cl^{-} (mg/L)	$SO4^{2-}$ (mg/L)
	<0.003	<0.0005	9	0.9	2.52	56.1
Parameters	Total dissolved solids (mg/L)	Alkalinity ($CaCO_3$)	pH	Hardness (mg/L $CaCO_3$)	Conductivity (μS/cm)	Caustic Soda Dose (NaOH) (mg/L)
	193	110	7.8	165	350	<20

Sand is unground silica sand from U. S. Silica Company, Ottawa. The size of sand was AFS (American Foundrymen's Society) 50-70 mesh (300μm-212μm). The main

properties and micrograph of the silica sand are shown in Table 3-4 and Figure 3-2, respectively.

Table 3-4 Main properties of the silica sand

Color	Grain shape	Hardness (Mohs)	Specific gravity (g/cm^3)	Mineral	Chemical analysis
white	round	7	2.65	Quartz	SiO_2 99.7%

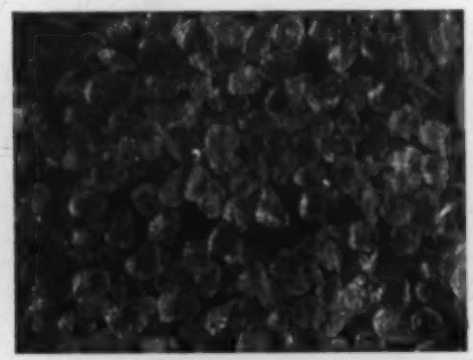

Figure 3-2 Micrograph of silica sand particles

3.3 Experimental setup/apparatus

3.3.1 Potentiodynamic measurement setup

Polarization curves of A1045 carbon steel in distilled water and 1M $NaHCO_3$ were performed in the three-electrode corrosion cell at room temperature with a potentiostat—Solartron SI1287, as shown in Figure 3-3. For all the electrochemical tests in this research, the test specimen is the working electrode, a platinum coil is the counter electrode and a saturated calomel electrode (SCE) is the reference electrode.

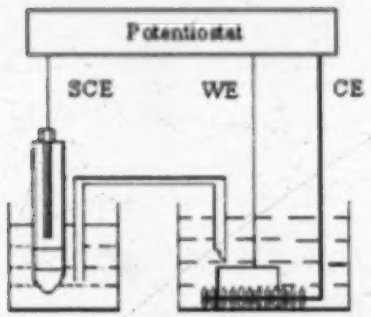

Figure 3-3 Corrosion cell used in potentiodynamic measurement

3.3.2 Micro-hardness tester

A micro-hardness tester was used in hardness measurement. Here, because the hardness test was conducted under polarization conditions, one self-designed corrosion cell was used to contain the solution and work piece. The electrochemical cell was fixed on the moving stage of the micro-hardness tester by bolts. The specimen also needs to be held tightly during the hardness test. Before testing, the specimen was glued on the electrochemical cell, which ensures that the specimen will not move during the test and also ensures that the test surface is perpendicular to the indenter.

Anodic polarization tests were performed in the three-electrode corrosion cell at room temperature. The applied anodic polarization currents were controlled by EG&G potentiostat. The Vickers micro-hardness of steel samples was measured with the set-up shown in Figure 3-4.

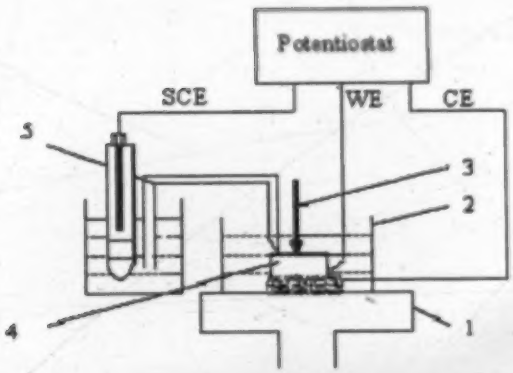

Figure 3-4 Schematic illustration of the micro-hardness measurement system
1—Movable Stage; 2— Electrolyte Cell; 3—Load; 4—Specimen; 5— Salt bridge
WE: Working Electrode; CE: Counter Electrode; SCE: Saturated Calomel Electrode

3.3.3 Rotating cylinder electrode (RCE)

For the electrochemical measurements in the erosion-corrosion test, a modified rotating cylinder system was used, as shown in Figure 3-5. The corrosion cell has 140 mL capacity with an inner diameter of 51.6 mm and height of 76 mm. A plastic cover was put on the cell and there was an O-ring between the cover and the cell to avoid eroding particles and electrolyte from spilling out. The platinum counter electrode coil was placed near the bottom of the corrosion cell. The SCE was placed outside the corrosion cell to avoid affecting the flowing conditions. SCE was connected to the cell with a Luggin capillary.

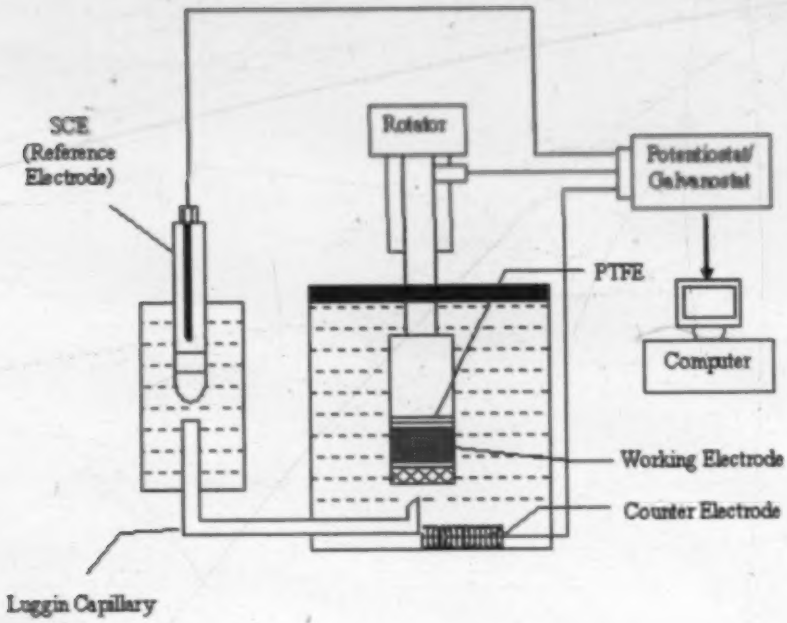

Figure 3-5 Schematic illustration of the electrochemical measurement apparatus

The rotating cylinder electrode (A1045 carbon steel) was mounted in the middle section of the E3M shaft, driven by a Pine ARMSRX analytical rotator, which is the preferred electrode rotator for use in the research laboratory. The rotation rate of the electrode may be precisely controlled using a four digit pushbutton control. The rotation rate is adjustable to within 1% of the control setting over a range from 50 to 10000 RPM. When the rotator rotates, water and sand are lifted up from the bottom and flow through the gap between the specimen and the cylinder. Electrical contact was made via four springs with silver carbon contact brushes connected to the rotating shaft.

For the weight loss measurement, the experimental apparatus was almost the same as used in the electrochemical measurement. The cell had the same size as the electrochemical cell. The differences are that the rotating electrode was driven by a Talboy stirrer. The rotating range was 50-7500 RPM. The shaft was a stainless steel shaft. Before testing, the rotating speed of the stirrer was calibrated by using an optical tachometer.

3.4 Experimental procedures

3.4.1 Preparation of the samples

For hardness testing, the test specimen was mounted in epoxy with a connecting wire come out from the arm side. One surface was exposed. The surface and bottom of the specimen must be flat and parallel to ensure the test surface is perpendicular to the indenter. The surfaces of each of the specimen for micro-hardness testing were ground on silicon carbide paper starting with 240 grade and finishing on 600 grade. Next, they were polished with 6 micron grade diamond paste on Metron B cloth, and then polished with 1 micron fine magnesia and 0.05 micron aqueous fine alumina successively. After finish polishing, thorough washing was followed by drying off with acetone or alcohol.

For erosion-corrosion testing, the grinding and drying processes of the cylindrical surface were the same as the hardness test samples. The top and bottom surface were painted with lacquer before the experiment to prevent crevice corrosion.

3.4.2 Hardness test procedures

The Vickers micro-hardness of steel samples was measured with an indenting load of 200 g while a constant anodic current was applied. Loading time was 15 seconds.

3.4.3 Erosion-corrosion test procedures

The experiments were carried out with different sand concentrations and flow rates for both electrochemical and erosion-corrosion measurements. Temperature was not controlled in the experiments.

3.4.3.1 Electrochemical test--Potentiodynamic polarization method

Polarization curves were determined by the potentiodynamic sweep method with a potentiostat—Solartron SI1287. After the open circuit potential was stabilized,

polarization curves were measured, which involves shifting the electrode potential of a working electrode at a predetermined rate (0.166mV/s). As the potential was shifted, current was monitored between the corroding working electrode and the inert counter electrode-platinum wire.

The corrosion current density i_{corr} was obtained by the Tafel method. For reactions that are activation controlled, the current density can be expressed by the Tafel equation.[72]

$$\eta = \pm\beta \log \frac{i}{i_{corr}} \qquad (3\text{-}1)$$

Where η is the overpotential, $\eta = E_{applied} - E_{corr}$, mV.

β is the Tafel slope, mV.

β_a is the anodic Tafel slope, mV.

β_c is the cathodic Tafel slope, mV.

i is the measured current density, A/m^2.

i_{corr} is the corrosion current density, A/m^2.

The Tafel slope for the anodic and cathodic reactions occurring at open circuit can be obtained from the linear regions of the polarization curve, as shown in Figure 3-6.[72] Extrapolate back from the anodic and cathodic regions to the point where the anodic and cathodic currents are equivalent. The current density at that point is the corrosion current density (i_{corr}). The corresponding potential at that point is the corrosion potential (E_{corr}).

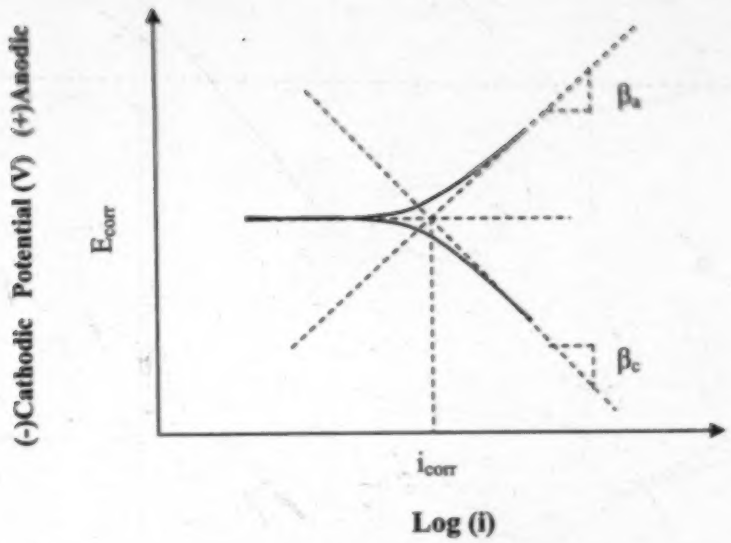

Figure 3-6 Tafel slope calculation[72]

3.4.3.2 Weight loss test

The total weight loss (*TWL*) was measured in the slurry with various flow rates. It encompasses all the possible degradation mechanisms involving electrochemical processes, mechanical effects and synergistic effects. Pure corrosion rates were measured in flowing tap water with various flow rates. The initial and final mass of each specimen was measured with an analytical balance with an accuracy of 0.1 mg.

In order to measure the pure erosion rate, the specimen was cathodically protected. An external power supply with -0.85V vs. SCE was applied between the specimen and the platinum electrode.[73,74] Specimen preparation procedures in cathodic protection were the same as those for the erosion-corrosion test except that they were not painted with lacquer.

Weight loss test under anodic polarization was conducted by a DC power supply with a high resistor to supply a constant current. By this method, the relationship between synergy and corrosion current density can be obtained.

All corrosion products and foreign matter on the specimen surface must be removed before the final weight was measured. According to ASTM G1-90,[75] hydrochloric acid + hexamethylene tetramine (inhibitor) solution was used in the experiments to remove the corrosion product. Acetone was used to remove the lacquer. Then the test piece was cleaned with de-ionized water, ethanol and dried with filtered dry air. The final mass was measured.

3.4.3.3 Surface morphology analysis

The surface morphology of the specimens was analyzed by an optical microscope and SEM. More than 10 pictures were taken in different locations on each of the specimen surfaces obtained in different test conditions. Image-pro plus software was used to analyze these pictures and then to quantify the size and area fraction of the wear scars and pits.

Chapter 4 Results and discussions

4.1 Hardness degradation due to chemo-mechanical effect

4.1.1 Effect of anodic dissolution on surface hardness

The relationships between hardness drop ($\Delta Hv / Hv_0$) vs. applied anodic current density for A1045 carbon steel under anodic polarization condition in distilled water and 1M $NaHCO_3$ solution are shown in Figure 4-1, where the change of hardness ($\Delta Hv = Hv - Hv_0$) is normalized with the original hardness (measured without applying anodic current) Hv_0.

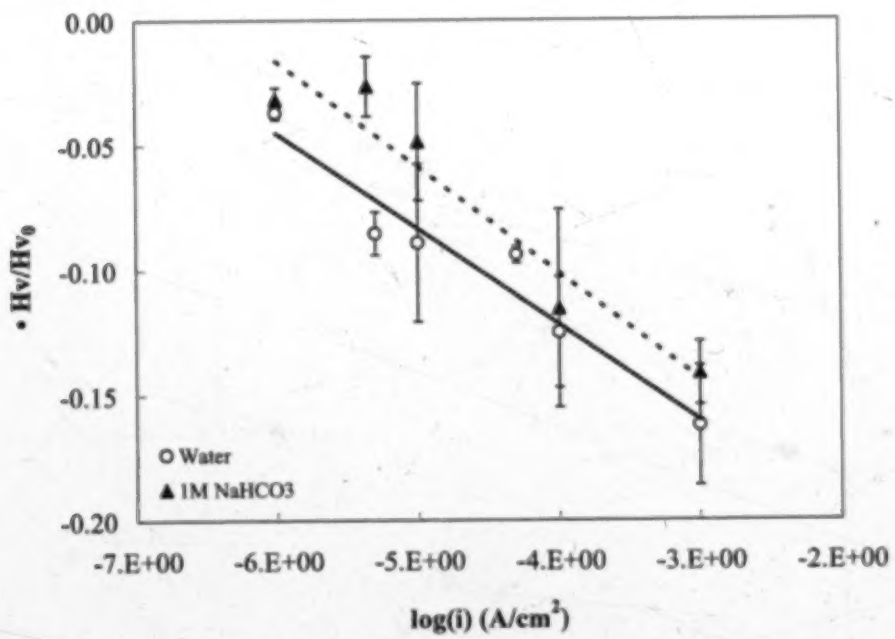

Figure 4-1 Hardness drop vs. anodic current density

The results show clearly that the hardness of material decreases with the increase of anodic dissolution current density and the hardness drop is proportional to the logarithm of anodic polarization current density for the test solutions adopted. Although

the test material displays quite different dissolution behavior in the two test solutions, the dependence of the hardness on the anodic current density is similar. It implies that the hardness degradation is mainly controlled by the anodic current density but is independent of the polarization behavior. Figure 4-2 is the potentiodynamic curves of A1045 in distilled water and 1M $NaHCO_3$ solution, which shows that A1045 carbon steel displays an active dissolution behavior in distilled water and an active-to-passive transition (self-passivating) behavior in 1M $NaHCO_3$ solution.

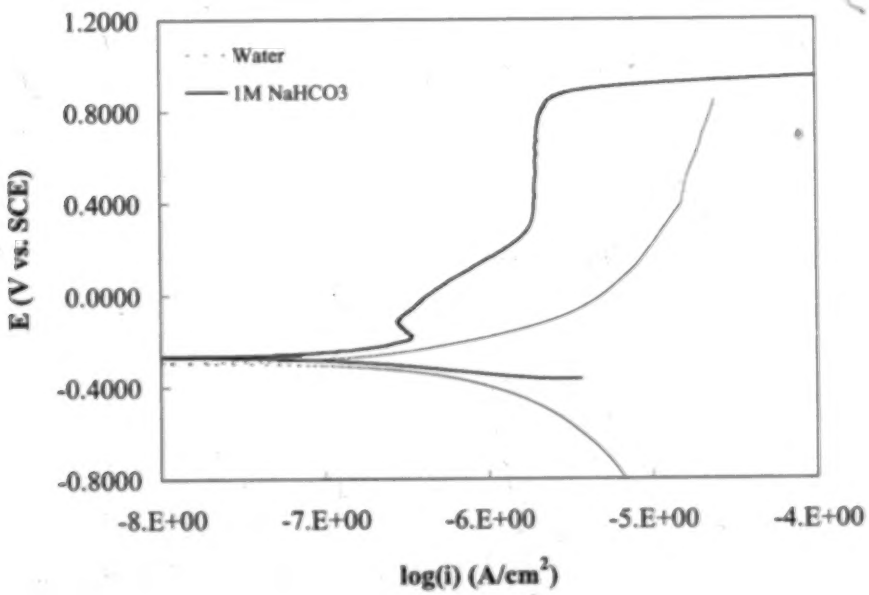

Figure 4-2 Polarization curves of A1045 in distilled water and 1M $NaHCO_3$ solution

The correlation between the normalized hardness drop ($\Delta Hv / Hv_0$) can be formulated as a linear function of the logarithm of anodic current density:

$$\frac{\Delta Hv}{Hv_0} = -\lambda \log\left[\frac{i}{i_0}\right] \qquad (4\text{-}1)$$

Where λ (>0) and i_0 are the constants determined by experiments. Here, λ=0.04, i_0=5.62E-7A/cm^2. The parameter i_0 can be recognized as a threshold current density beyond which the chemo-mechanical effect is observed.

According to Figure 4-1, the normalized hardness drop ($\Delta Hv / Hv_0$) is a linear function of the logarithm of current density, which is in good agreement with the experimental results reported by Gutman.[75,76] These results imply that the physical-mechanical properties of metals degrade with the occurrence of electrochemical or chemical reaction on surface. Gutman referred the hardness degradation phenomenon due to the presence of anodic dissolution on surface as to chemo-mechanical effect, which is discussed in next section.

4.1.2 Chemo-mechanical effect

It has been well known that the plastic deformation is resulted from the dislocation movement from one equilibrium location to the other location and the difference between soft and hard materials is mainly due to the differences in the mobility of their dislocations.[76]

The anodic dissolution of carbon steel can be considered as a continuous process but it is not a uniform process. Not all of the atoms, but only those with high energy on the surface, can leave the metal lattice. The atoms with high energy normally exist in the zones around crystalline defects, such as dislocation corners, plane edges, etc, as shown in Figure 4-3.[77] Atoms at the corner A and edge B have much higher energies than atoms in the positions C and D. The atoms with high energy have higher tendency to go into solution. It is expected that the stability of atoms increases in the series: A < B < C < D. The removal of these atoms by dissolution at these anodic points will produce new anodic sites.

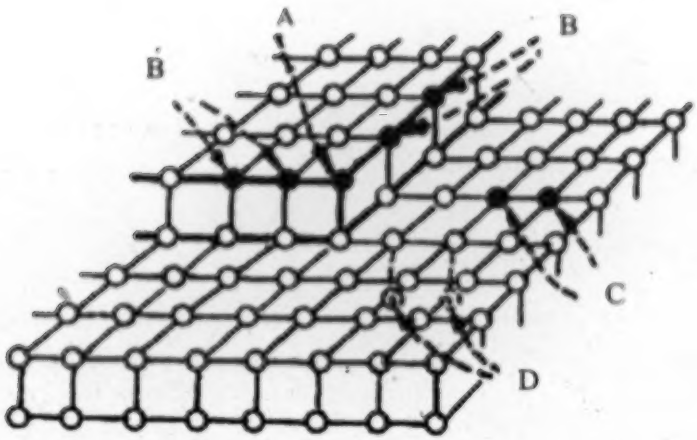

Figure 4-3 Schematic lattice structure of surface of a crystal material[77]

Gutman[59,60] described the physical meaning of the chemo-mechanical effect as follows. When anodic dissolution takes place, the metal atom must leave the metal lattice. A two-dimensional dissolution nucleus is formed with a mono-atomic depth. Subsequently, the etching of the mono-atomic layer step along the crystallographic plane causes the dissolution of crystals. New two-dimensional nuclei form continuously during the occurrence of dissolution. By this continuous and repeated dissolution process, the mono-atomic layer step is removed layer by layer, resulting in the continuous dissolution of metal. Because the mono-atomic layer step on the surface can serve as the source of new dislocations,[78] an additional dislocation flux forms during the anodic dissolution process because of the chemo-mechanical effect. This means that the formation of the dislocation flux is the result of heterogeneous surface dissolution.

Anodic polarisation causes an additional dislocation flux and the presence of dislocations increases the disorder and the entropy of the crystal and lowers the free energy, which makes it easier for the dislocation to move. With an increase in anodic current density, dislocation mobility is enhanced. The resistance to plastic deformation decreases. On a macroscopic scale, the yield strength of the surface material decreases and the surface material becomes soft.[59,60]

In addition, softening caused by the weakening of inter-atomic bonds as a result of dissolution of the surface layer leads to micro-stress relaxation and a decrease in the chemical potential of dislocations in this layer. The chemical potential gradient between the surface layer and the bulk material is likely to result in an additional dislocation flux and the dislocation will move to the surface layer. Because the mean free path of dislocations possesses a limited value, only the dislocations situated in the surface layer with a depth less than or equal to the mean free path can reach the surface,[60,77] so that the chemo-mechanical effect can only affect the mechanical properties in this surface layer.

4.2 Microstructure and hardness results after heat treatment

4.2.1 Microstructure

From iron-iron carbide phase diagram, a eutectoid reaction occurs as the austenite (γ) cools below 727 °C for steel.

$$\gamma\ (0.76\ \text{wt\% C}) \underset{\text{Heating}}{\overset{\text{Cooling}}{\rightleftharpoons}} \alpha\ (0.022\ \text{wt\% C}) + Fe_3C\ (6.67\ \text{wt\% C}) \qquad \text{(pearlite)}$$

Tempering and annealing can be accomplished by heating samples under different temperatures. At 500 °C, a tempered microstructure was obtained, while at 850 °C and 1050 °C, full annealed microstructures were obtained for A1045 carbon steel. 1050 °C is not a normal annealing temperature. We use it to obtain large grain size; therefore we can get low hardness.

The as-received, tempered and annealed microstructures at different temperatures of A1045 carbon steel are shown in Figure 4-4 (a), (b), (c) and (d), respectively.

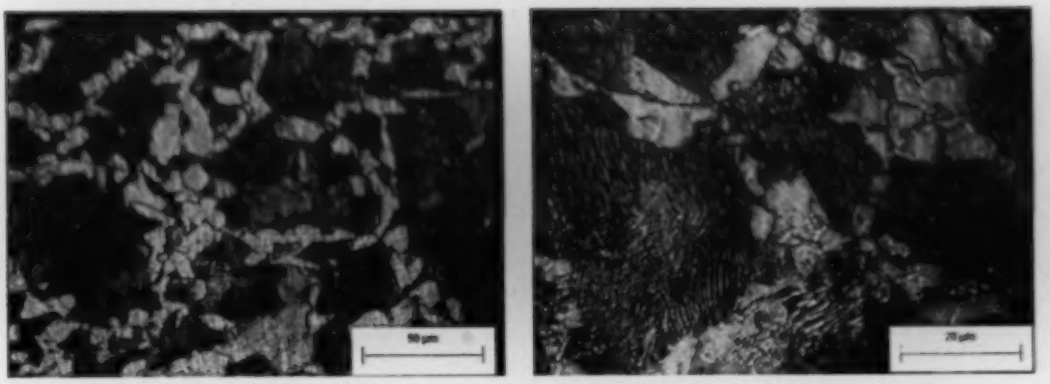

200x 500x

(a) A1045 carbon steel --as received

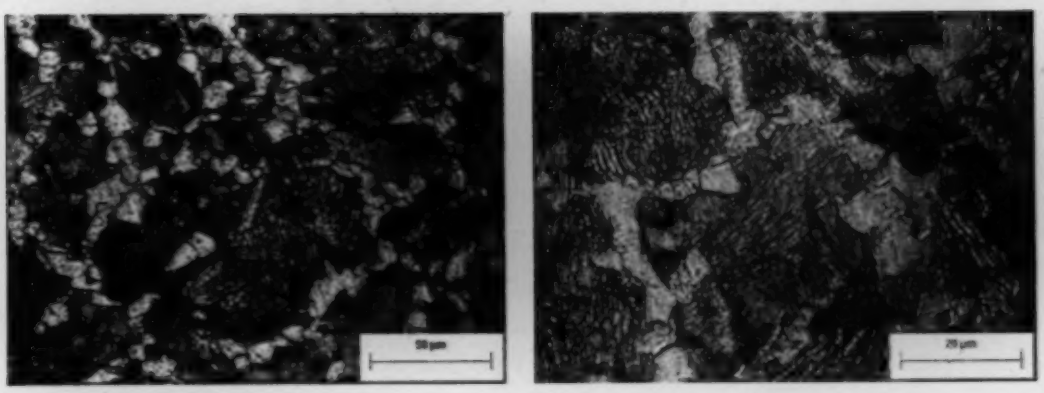

200x 500x

(b) A1045 carbon steel --500 °C tempered

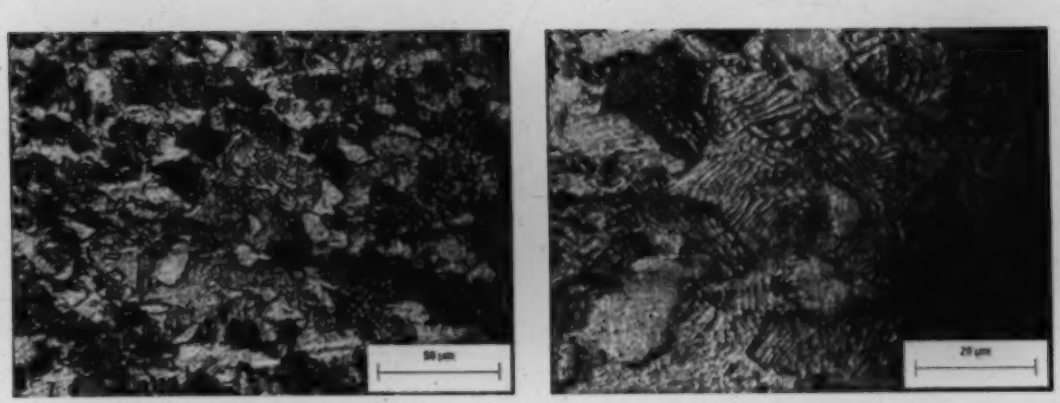

200x 500x

(c) A1045 carbon steel --850 °C annealed

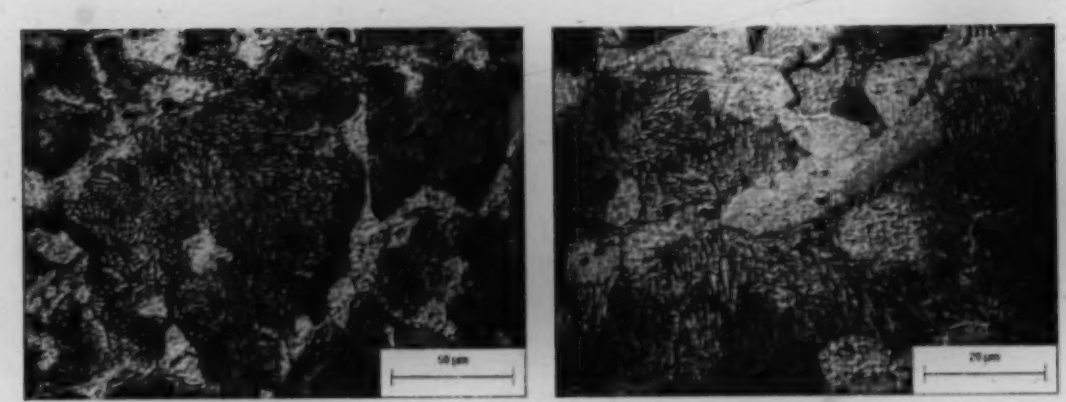

200x 500x

(d) A1045 carbon steel --1050 °C annealed

Figure 4-4 Photomicrograph of A1045 carbon steel under various heat treatment conditions

Comparing Figure 4-4 (a), (b), (c) and (d), all the microstructure products are pearlite and proeutectoid ferrite. The grain size and lamellar spacing of pearlite increase as the increase of heat treating temperature, which is more obvious in Figure 4-4 (d).

4.2.2 The relationship between hardness and heat treating temperature

The relationship between hardness and heat treating temperature is shown in Figure 4-5. We can see that hardness decreases with an increase in the heat treating temperature.

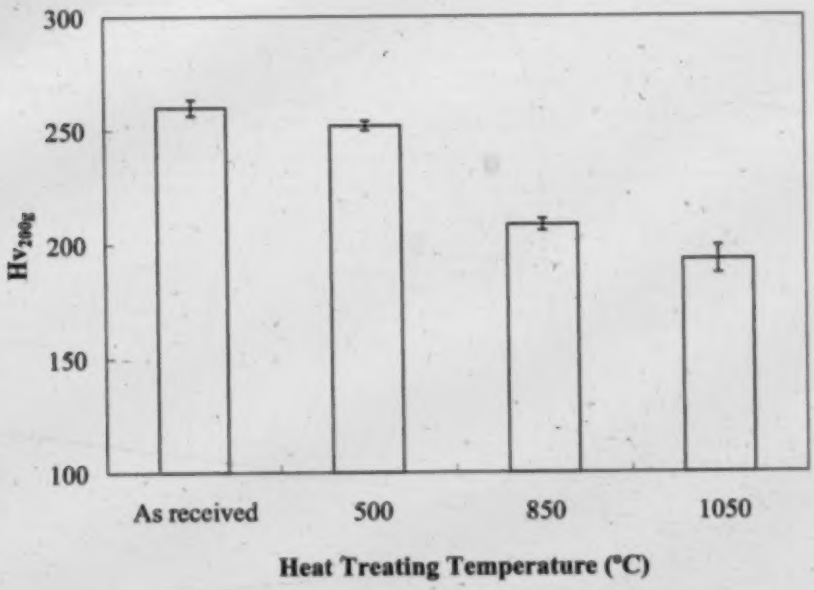

Figure 4-5 Relationship between hardness and heat treating temperature

The hardness under as received condition is the highest because the material was hot-extruded, which means that it was fabricated at an elevated temperature (i.e. austenite phase). Internal residual stress may develop in metal pieces in response to the following processes: (1) plastic deformation process; (2) non-uniform cooling of a piece that was processed or fabricated at an elevated temperature—heat stress; and (3) phase transformation that is induced upon cooling wherein parent (austenite) and product phases (ferrite and FeC_3) have different densities—structural stress.[77,79] For example, during the hot extrusion process of a steel rod, the deformation of the external circle is higher than that of the inside. The external surface has tensile stress, while the inside has pressure stress. Also during the plastic deformation process, plenty of dislocations are

generated. Some of the atoms deviate from the equilibrium position causing lattice distortion. Therefore internal residual stress develops because of plastic deformation process in metal pieces.[77]

After tempering and annealing, the hardness of A1045 carbon steel is lower than that of the as-received because heat stress and structural stress were relieved by tempering and annealing, during which recovery and recrystallization occur. A new set of strain free equiaxed grains that have low dislocation densities were formed.[77] Hardness of the material after a 1050 °C anneal is lower than that of an 850 °C anneal because the grain size and lamellar spacing of pearlite increase.

It is known that macroscopic plastic deformation corresponds to the motion of large numbers of dislocations. The ability of a metal to plastically deformation depends on the ability of dislocations to move. Restricting or hindering dislocation motion renders a material harder and stronger. Since grain boundaries act as barriers to dislocation motion, the smaller the grain size, the greater the grain boundary area, the harder and stronger is the material. For many materials, the yield strength σ_y is inversely proportional to the square root of grain size according to the *Hall-Petch equation*[79]

$$\sigma_y = \sigma_0 + k_y d^{-1/2} \qquad (4\text{-}2)$$

In this expression, d is the average grain diameter. σ_0 and k_y are material constants. σ_0 is approximately the yield strength of the single crystal material. α-Fe_3C phase boundaries also serve as barriers to dislocation motion in the same way as grain boundaries. Pearlite is a lamellar structure with ferrite and cementite (Fe_3C). Ferrite has good ductility, while Fe_3C is hard and brittle. The strong and rigid cementite phase severely restricts deformation of the soft ferrite phase in the regions adjacent to the boundaries; thus the cementite reinforces the ferrite. The degree of this reinforcement is higher in fine pearlite because of the greater phase boundary area per unit volume of material.[79]

4.3 Pure corrosion rate

4.3.1 Electrochemical test results--Potentiodynamic polarization

Potentiodynamic polarization scans were performed from the cathodic to the anodic direction at different flow rates in tap water. The polarization curves in tap water are shown in Figure 4-6.

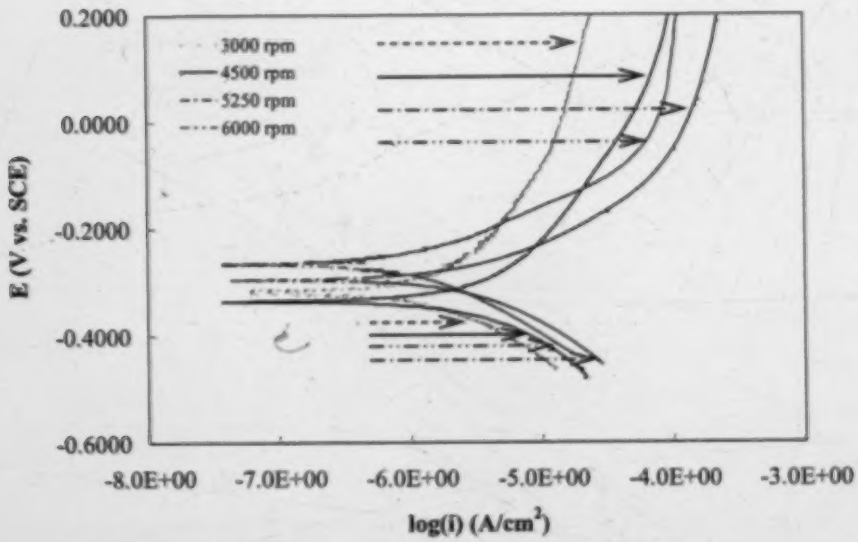

Figure 4-6 Potentiodynamic curves in tap water with various flow rates

From Figure 4-6, both of the anodic and cathodic reactions are accelerated with an increase of flow rate. Flowing liquid is helpful to remove the corrosion products, exposing fresh surface to corrosion; therefore, the anodic reaction is enhanced with the increase of flow rate. It has been well recognized that, in aerated, near neutral solution, the cathodic reaction is the reduction of O_2. This reaction is normally, at least partially, controlled by the mass transport of dissolved oxygen in the solution and such a process will be accelerated with increasing flow rate. Therefore, the cathodic reaction is also promoted with the increase of flow rate, as shown in the cathodic branch of Figure 4-6.

4.3.2 Weight loss test results

Weight loss tests were conducted in tap water under different flow rates to obtain the pure corrosive component. The relationship between the pure corrosion rate and flow rate is shown in Figure 4-7. It also verified that the corrosion rate increases with an increase of flow rate.

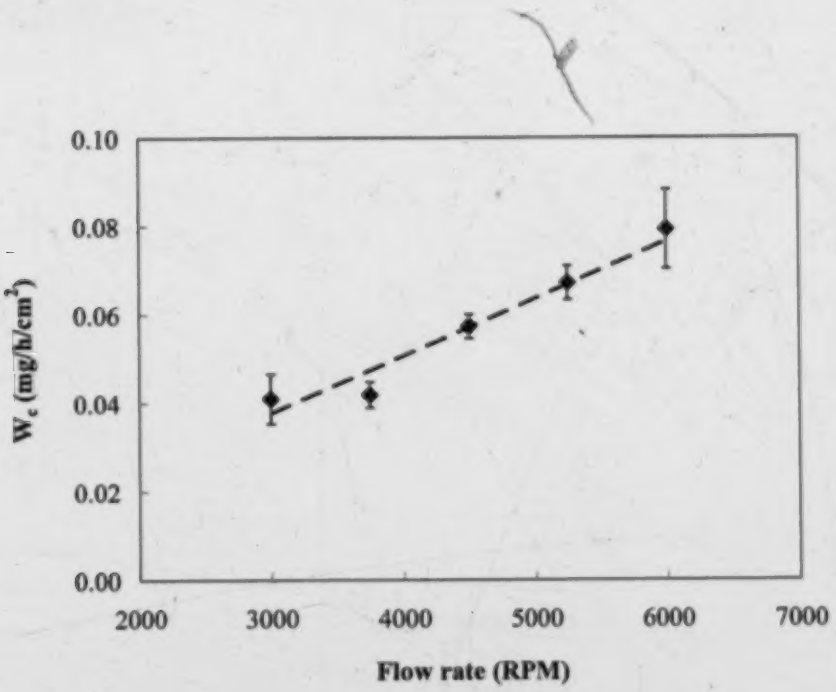

Figure 4-7 Dependence of the pure corrosion rate on flow rate

4.4 Pure erosion rate

4.4.1 Calibration of the weight loss test

Weight loss tests were conducted in flowing slurry. Three sets of comparing test were conducted to verify the validity of the weight loss test, i.e. dependence of weight loss on test duration, sand degradation and the effect of roughness of the sample surface. Slurry with 20 wt % sand at 7300 RPM under an applied anodic current density 1E-4

A/cm^2 was used to get a faster result. All three sets of tests were interrupted about every two hours to measure the weight loss of samples.

In the first set of tests, before the test was restarted, the sample was not polished; the surface roughness was allowed to develop. However, the sand was changed to new sand. In the second set of tests, before the test was restarted, the sample was not polished and the sand was not changed. In the third test, the sample was polished, but the sand was not changed. The results in Figure 4-8 show that, the relationship of weight loss and time duration is a linear function in the three conditions, which indicates that the use of weight loss per unit time is valid. Figure 4-8 also shows that the weight losses of the three samples are very close, indicating the influence of sand degradation and the surface roughness are very small.

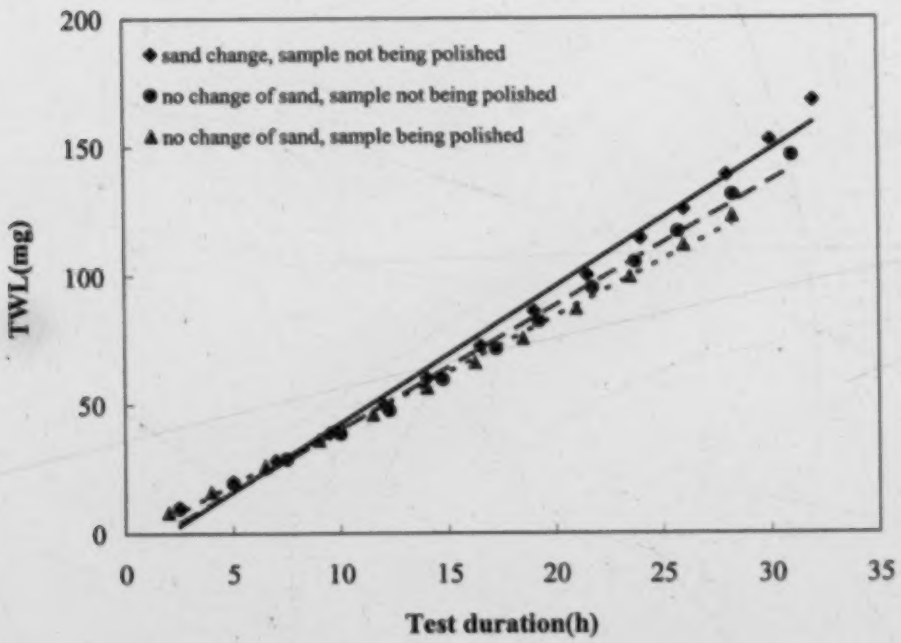

Figure 4-8 Comparing tests to verify the validity of weight loss test

4.4.2 Pure erosion rate

The dependence of the pure erosion rate on flow rate and sand concentration is shown in Figure 4-9. The results indicate that the pure erosion rate increases with the increase of flow rate and sand concentration in the test conditions adopted.

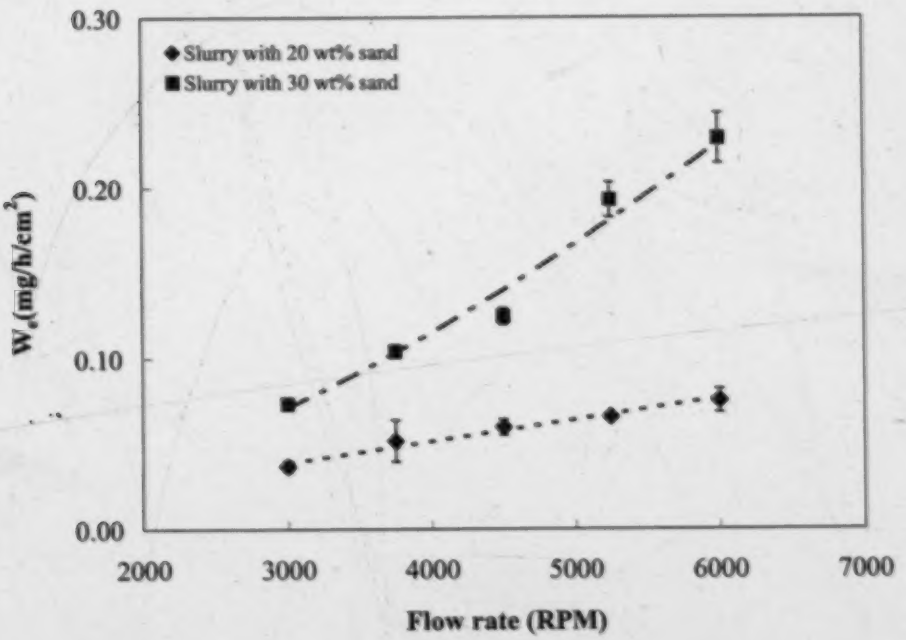

Figure 4-9 Dependence of the pure erosion rate on flow rate and sand concentration

4.5 Synergy between erosion and corrosion

4.5.1 Electrochemical test results

Potentiodynamic polarizations were conducted in slurry containing 20 wt% and 30 wt% sand with various flow rates, as shown in Figure 4-10 and Figure 4-11, respectively. The polarization curves in slurry with various sand concentrations at the flow rate of 3000 RPM are shown in Figure 4-12.

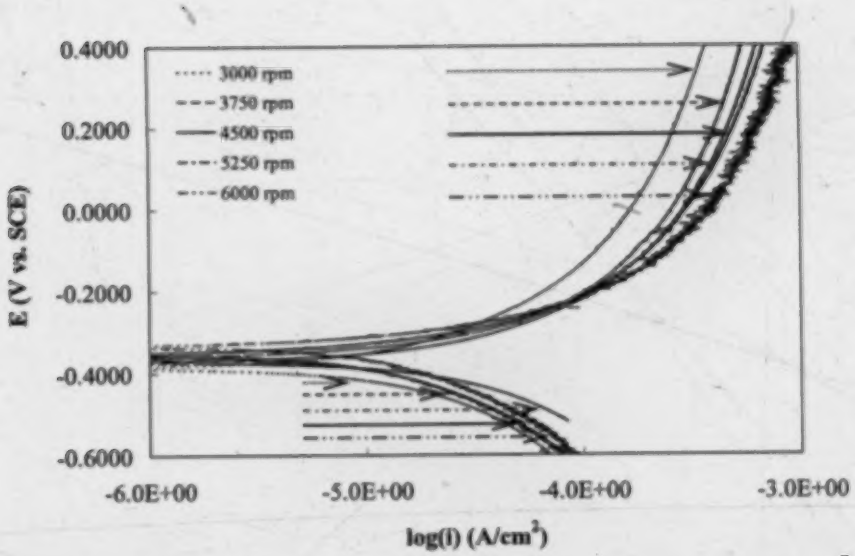

Figure 4-10 Potentiodynamic curves in slurry with 20 wt% sand under various flow rates

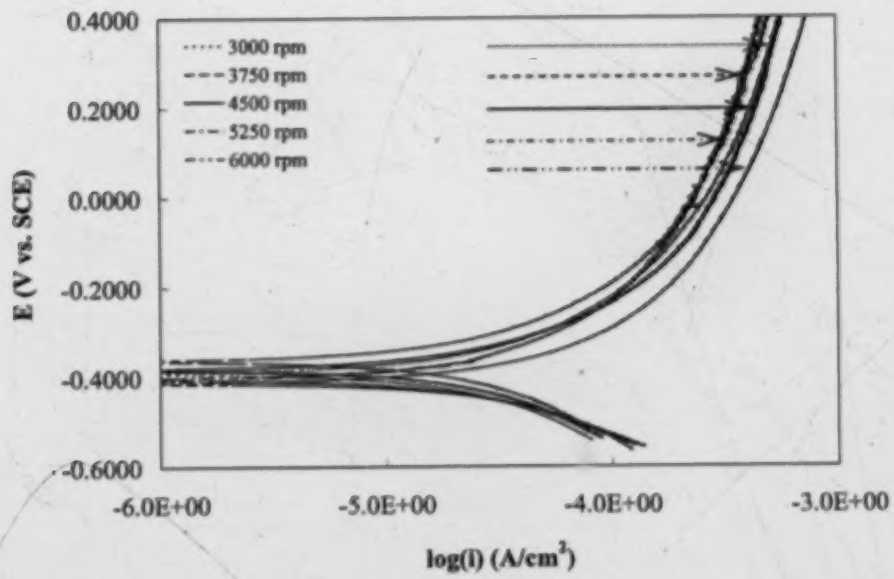

Figure 4-11 Potentiodynamic curves in slurry with 30 wt% sand under various flow rates

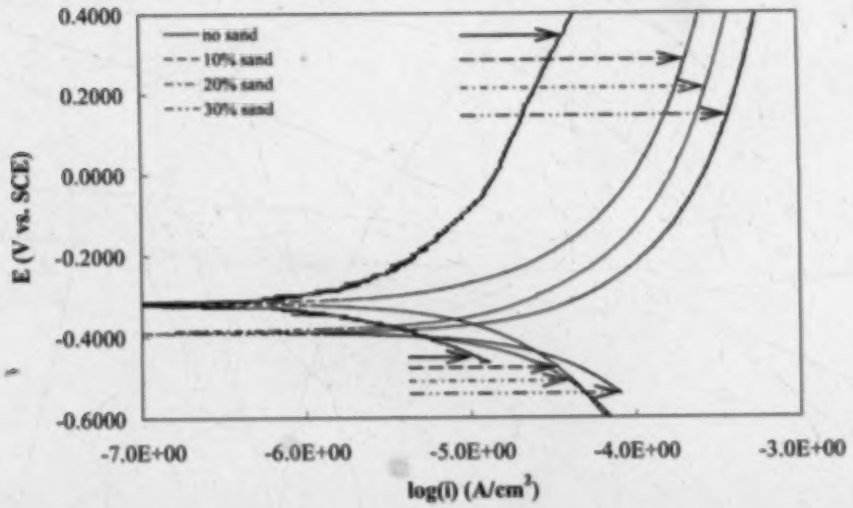

Figure 4-12 Potentiodynamic curves at 3000 RPM under various sand concentrations

From Figure 4-10 to Figure 4-12, both of the anodic and cathodic reactions are accelerated with an increase of flow rate and sand concentration. This indicates that the corrosion process in a slurry condition is a mixed control process. It is consistent with the result of C.H. Wu.[80] The reasons for the increase of corrosion rate with flow rate have been explained before. Here, the effect of sand impingement is analyzed.

In a slurry condition, there are two main causes responsible for this acceleration of the anodic dissolution. First, the probability of sand impingement increases with the increase of the flow rate and sand concentration. It is helpful to remove corrosion product to make fresh metal surface expose to corrosive medium.[43,44] Second, the impingement of sand particles on the electrode surface produces plastic deformation, causing more defects in surface layer.[51] Therefore, the material surface becomes more electrochemically active under erosion slurry condition.

As mentioned before, the cathodic reaction is the reduction of O_2 in an aerated, near neutral solution. Erosion helps remove the corrosion product on the surface. In addition, sand impingement also disturbs the interface of the Fe/electrolyte and promotes the diffusion of dissolved oxygen in the surface layer of the electrolyte, resulting in the acceleration of the cathodic reactions.[44,45] Therefore, the cathodic reaction is slightly

promoted with an increase in flow rate and sand concentration, as shown in the cathodic branch of Figure 4-10 to Figure 4-12.

To present these relationships more clearly, corrosion rate versus flow rate at various concentrations are summarized in Figure 4-13 . The corrosion rate is evaluated based on corrosion current density i_{corr}, which is calculated by extrapolating the Tafel lines to E_{corr}. From the electrochemical method, we can see the effect of erosion on corrosion, which is one form of synergy.

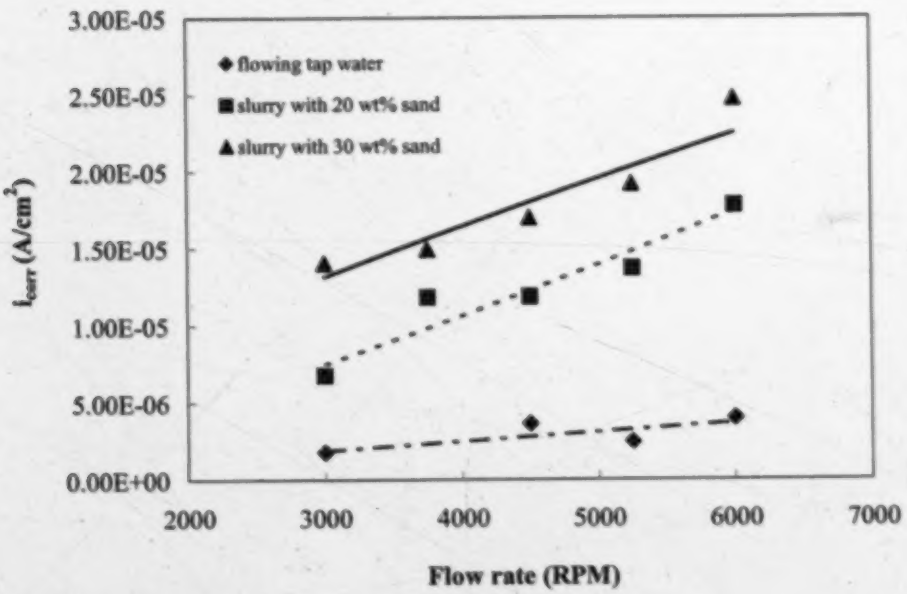

Figure 4-13 Effect of flow rate and sand concentration on i_{corr}

4.5.2 Contribution of each wastage component on erosion-corrosion

When the pure corrosion rate and pure erosion rate were deducted from the *TWL*, the synergy component between erosion and corrosion was obtained. The differentiation of each of the wastage components in slurry with 20 wt% and 30 wt% sand are shown in Figure 4-14 and Figure 4-15, respectively.

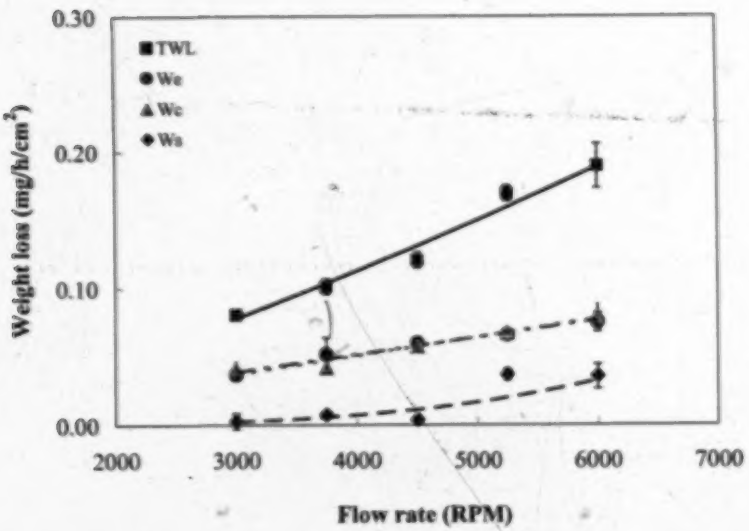

Figure 4-14 Differentiation of each of the wastage component as a function of flow rate in slurry with 20 wt% sand

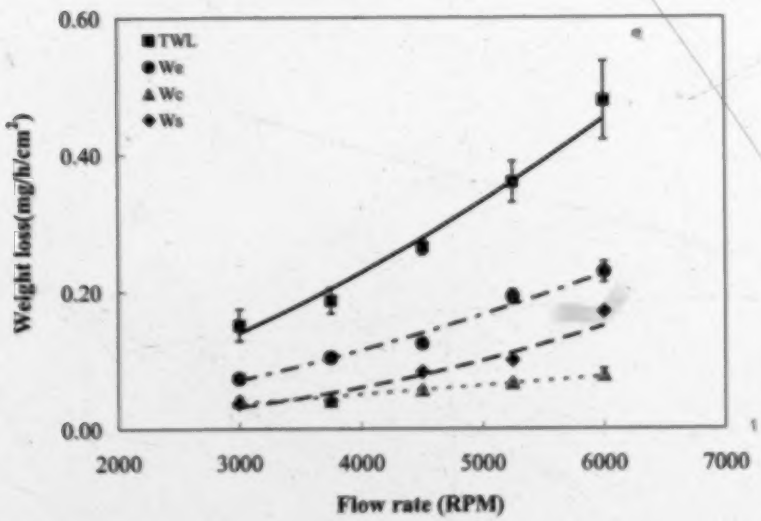

Figure 4-15 Differentiation of each of the wastage component as a function of flow rate in slurry with 30 wt% sand

The results indicate that *TWL* rate, pure corrosion rate (w_c), pure erosion rate (w_e) and synergy (w_s) increase with the increase of flow rate and sand concentration in the conditions studied. In the 20 wt% slurry condition, corrosion (w_c) and erosion (w_e) are the most important components in total weight loss. Synergy is not obvious. In the 30 wt% slurry condition, the synergy effect increases with the increase of sand concentration.

The fraction of synergy in slurry with 30 wt% sand under an open circuit condition at 3000 RPM and 6000 RPM are shown in Figure 4-16 and Figure 4-17, respectively. The fraction of synergy increases with the increase of flow rate and sand concentration because the interaction between erosion and corrosion increases with the increase of flow rate and sand concentration. In the 30 wt% sand slurry condition, it can reach as high as 36% of the *TWL*.

Figure 4-16 Fraction of each wastage component in slurry with 30 wt% sand at 3000 RPM

Figure 4-17 Fraction of each wastage component in slurry with 30 wt% sand at 6000 RPM

4.6 Mechanism of the synergy

4.6.1 Chemo-mechanical effect in erosion-corrosion process

4.6.1.1 Effect of hardness on mechanical erosion rate

Erosion-corrosion tests were conducted under cathodic protection with specimens of different hardness obtained by heat treatment. The effect of hardness of materials on the mechanical erosion rate (w_e) is shown in Figure 4-18. The results indicate that the material loss rate due to mechanical erosion increases as the hardness of the steel is reduced. The obtained result for this experiment agrees with other researchers work.[11,81] This can be explained by the material's resistance to plastic deformation decreasing with a decrease in hardness. It is known that a hardness test measures the resistance of a metal to plastic flow. During the hardness test, indentation takes place by plastic deformation in

metals. The plastic deformation is constrained by the elastic material surrounding it. The harder the material, the more difficult is plastic deformation. The erosion mechanism for ductile metals consists of a sequential plastic deformation process. Therefore, the erosion rate increases as hardness decreases.

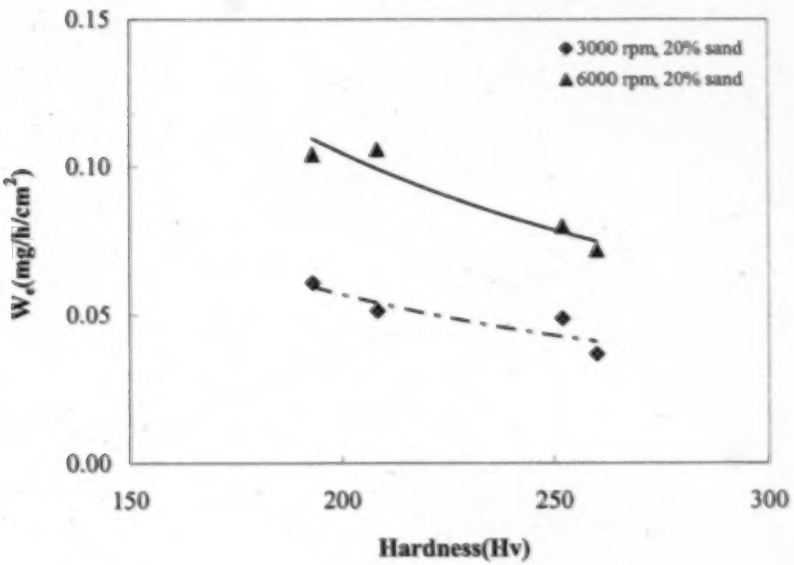

Figure 4-18 Dependence of mechanical erosion rate on hardness in slurry with 20 wt% sand

As mentioned before, some researchers[3,52] did not find a correlation between the hardness and the erosion-corrosion resistance. It is believed that such a relation depends on the contributions of corrosion-related components on the total material loss in the erosion-corrosion processes. If the corrosion-related mechanisms dominate the erosion-corrosion processes, it will be unlikely to find a dependence of total material loss on the hardness of the material.

In most of the erosion models, the erosion rate is a power function of the hardness of the material.[15,18,20] Under the current test condition, the dependence of the material loss

rate due to mechanical erosion (w_e) on the hardness shown in Figure 4-18 can be approximately formulated as follows

$$w_e = \alpha H v_0^{-\beta} \tag{4-3}$$

Where α and β (>0) are the constants determined by experiments. It is estimated that α is between 40 and 80, β is 1.26.

In light of the results in Figure 4-1 and Figure 4-18, the degradation in the erosion resistance is expected when corrosion current increases. Since the corrosion process can be promoted due to the existence of the erosion in erosion-corrosion process, as shown in Figure 4-13, hardness will degrade because of the corrosion effect. Therefore, the synergistic effect is expected owing to the hardness degradation in the erosion-corrosion process.

4.6.1.2 Chemo-mechanical effect in erosion-corrosion process

When an erosion-corrosion test is conducted under a galvanostat condition, dissolution is controlled. In line with the concept of the chemo-mechanical effect, the hardness of steel will decrease while anodic dissolution occurs on the surface, resulting in the degradation of erosion resistance. This means that equation (2-12) is still valid. The correlation between the value of w_s and corrosion current density can be obtained. The increment of erosion rate due to the presence of anodic dissolution is defined here as the synergy.

$$\Delta w_e = w_s \tag{4-4}$$

In line with Equation (4-3), when the flow rate keeps constant, we have

$$\Delta w_e = w_s \approx -\alpha\beta Hv_0^{-\beta-1}\Delta Hv = -\alpha\beta Hv_0^{-\beta}\left(\frac{\Delta Hv}{Hv_0}\right) \qquad (4\text{-}5)$$

Inserting Equation (4-1) into Equation (4-5), Equation (4-5) can be rewritten as follows,

$$\Delta w_e = w_s \approx -\alpha\beta Hv_0^{-\beta-1}\Delta Hv = -\alpha\beta Hv_0^{-\beta}\left(-\lambda \log\left[\frac{i}{i_0}\right]\right) = \beta\lambda w_e \log\left[\frac{i}{i_0}\right] \qquad (4\text{-}6)$$

So we get

$$\frac{w_s}{w_e} = \beta\lambda \log\left[\frac{i}{i_0}\right] \qquad (4\text{-}7)$$

The normalized synergy rate (w_s/w_e) will increase with increasing anodic dissolution rate and the relationship between them can be approximately formulated as a linear function of the logarithm of anodic current density. It was confirmed by the erosion test data in Figure 4-19, obtained under action of applied anodic current in slurry with 20 wt % sand. This indicates that erosion is enhanced by the chemo-mechanical effect when corrosion occurs simultaneously. From Figure 4-19, w_s/w_e decreases with the increase of flow rate, which shows that w_e is more sensitive to flow rate than w_s.

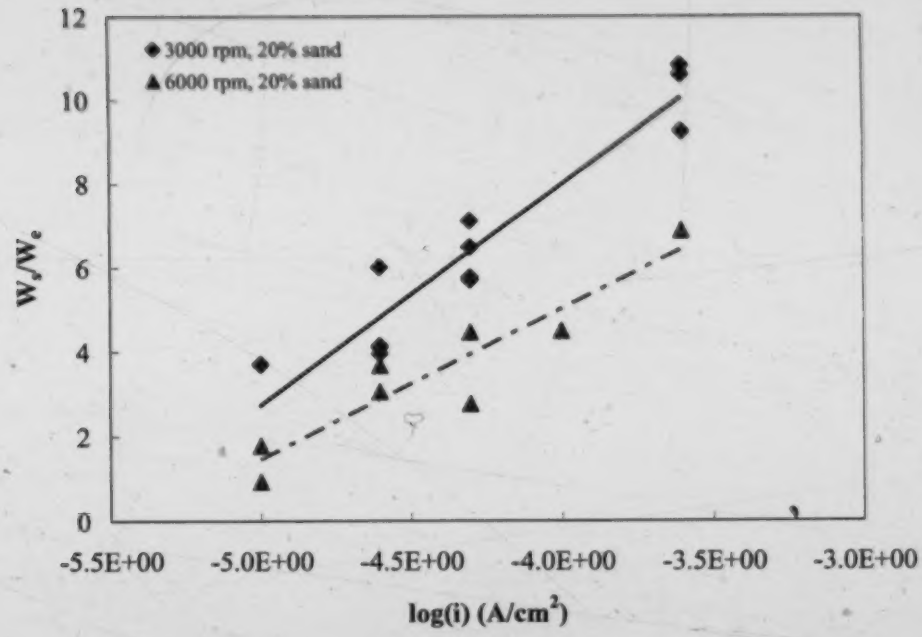

Figure 4-19 Dependence of the normalized synergy rate (w_s/w_e) on the anodic current density in slurry with 20 wt% sand

Suppose that the synergy is caused by the degradation of the mechanical erosion resistance because of the chemo-mechanical effect. According to the data in Figure 4-18, the exact value of w_s can be determined by substituting λ , i_0 and β into Equation (4-7). As mentioned before, λ =0.04, i_0 =5.62E-7A/cm^2, β =1.26. When the anodic current density rises to 2.5x10^{-4} A/cm^2, the normalized hardness drop will result in the increase of the erosion rate by about 13.3%. This value is much lower than the experimental measured value of w_s/w_e , which reaches as high as 10. This means that hardness degradation by chemo-mechanical effect is not the main reason caused the synergy.

The probable reasons behind it are analyzed as follows.

(1) Because of limitations of the measuring technique, the load used in the hardness measurement is too high and the depth of indentation is much greater than those of wear scratches produced by sand particle impingements, while the anodic current on

the surface can only affect the mechanical properties of a very thin layer on the specimen surface.

(2) The hardness degradation produced by the chemo-mechanical effect is not enough to account for the synergy. Other material loss mechanisms exist simultaneously. For example, pitting is obvious on the specimen surface after erosion-corrosion test. The material loss of carbon steel from the erosion-corrosion is non-uniformly distributed. The surface morphology after an erosion-corrosion process will be analyzed next.

4.6.2 Damage of surface morphology due to erosion-corrosion

In order to understand the mechanism of synergy, the surface morphology of a specimen was analyzed after the erosion-corrosion tests. Figure 4-20 is the surface before the erosion-corrosion test, which will be used for comparison.

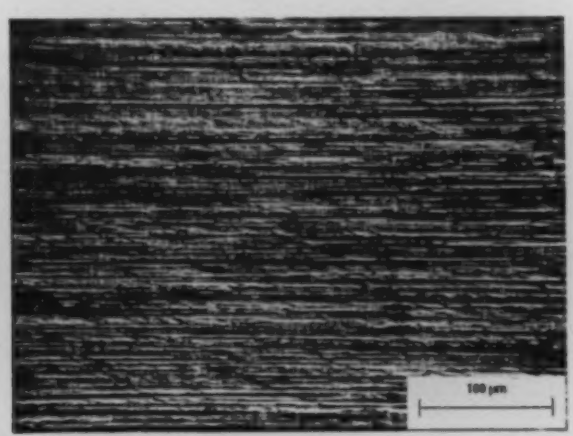

Figure 4-20 Surface morphology of the specimen before erosion-corrosion test

4.6.2.1 Surface morphology in tap water

Surface morphology after static immersion in tap water for 30 minutes under open circuit potential is shown in Figure 4-21 (a). Uniform corrosion and some corrosion pits were found on the surface. Considering the two-phase microstructure of the test material,

the surface was polished and etched. It is found that most of the pits occurred on the pearlite or grain boundaries of proeutectoid ferrite and pearlite, as shown in Figure 4-21 (b).

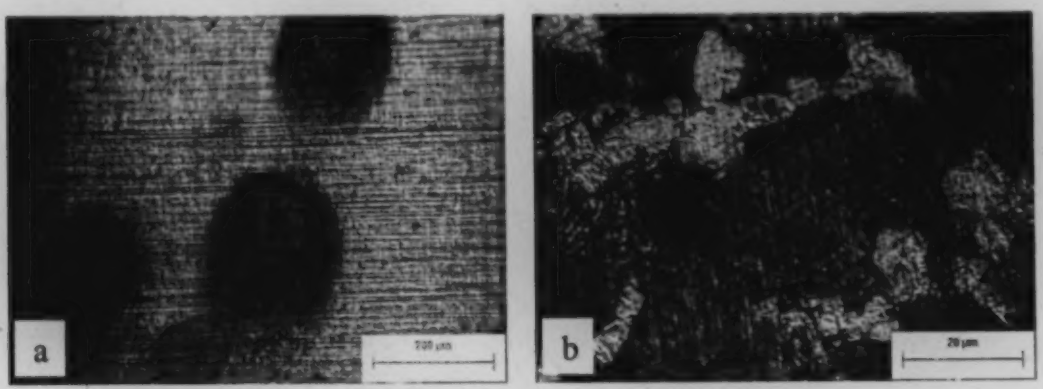

Figure 4-21 Surface morphology after static immersion in tap water
30 minutes, under open circuit condition
(a) Surface morphology after immersion (b) Corrosion pits after polishing and etching

It is known that corrosion resistance depends on the microstructure and the distribution of alloying elements. In general, a single-phase microstructure has higher corrosion resistance than multi-phases. Pearlite is composed of Fe_3C and ferrite. Fe_3C has a lower potential than ferrite,[82] so micro-galvanic cells form between Fe_3C and ferrite.[63] Ferrite is the cathode, Fe_3C is the anode. Selective attacks occur at and around pearlite bands. Some investigators[83,84] also believe that steels containing fine pearlite corrode more rapidly than those with coarse pearlite, which means that corrosion increases as the pearlite lamellar spacing of Fe_3C decreases because of the increase of contact area between the pearlite and ferrite. Corrosion rate also increases with an increase in carbon content.[84]

Figure 4-22 shows the surface morphology in flowing tap water under an open circuit condition for 30 minutes at 6000 RPM. We can see some corrosion pits on the surface. The pit number is a little bit higher than that under the static immersion condition in tap water as shown in Figure 4-21 (a).

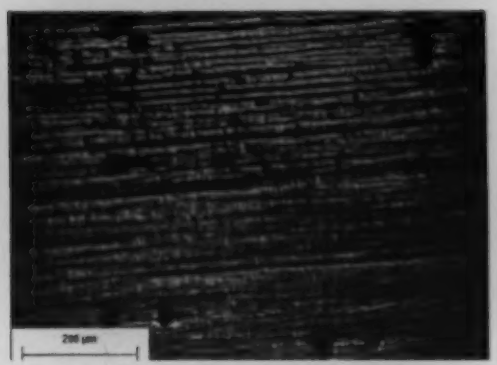

Figure 4-22 Surface morphology in tap water under open circuit condition
30 minutes, 6000 RPM

4.6.2.2 Surface morphology under cathodic protection condition

Figure 4-23 (a) and (b) are the surface morphology after static immersion in tap water for 30 minutes under cathodic protection. When the specimen was taken out from the water, lots of deposited particles were seen on the surface, but no corrosion pits were found, as shown in Figure 4-23 (a). The deposited particles can be easily removed. Figure 4-23 (b) shows the surface of the specimen after the deposited particles were removed. XRD analysis in Figure 4-24 shows that the composition of the deposit is mainly $CaCO_3$.

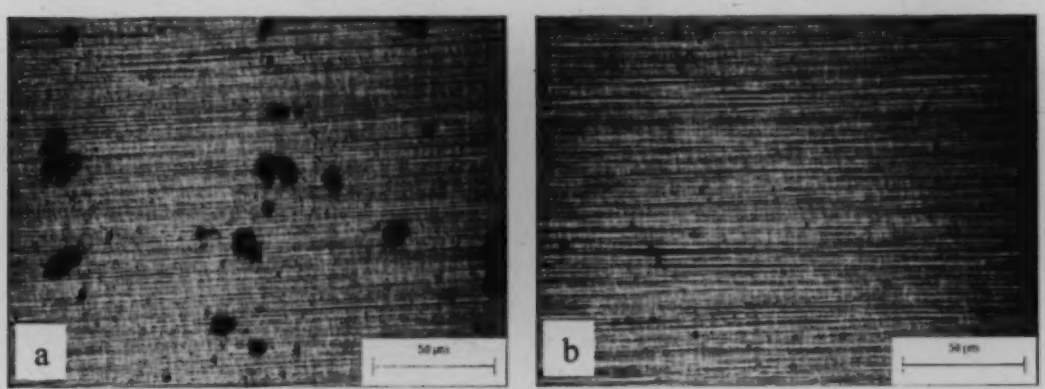

Figure 4-23 Surface morphology after static immersion in tap water for 30 minutes under cathodic protection
(a) Deposited particles (b) Deposited particles being removed

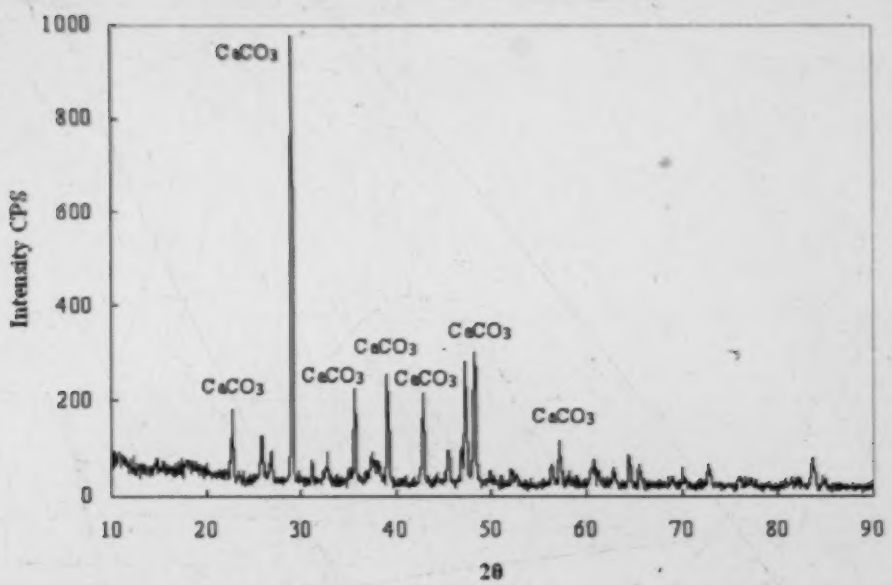

Figure 4-24 XRD result of the deposit—composed by $CaCO_3$

In the RCE system, the erosion of a metal surface results from the dynamic action of moving particles. Figure 4-25 (a) and (b) are the surface morphology for the specimens after testing for 30 minutes under cathodic protection in flowing slurry at 6000 RPM (with 10 wt% and 20 wt% sand, respectively). Clear wear scars (due to chipping) and plastic deformation (raised material lips) at the side and the exiting rim of the long grooves are found from the impact of solid particles. No corrosion pits are found. Plastic deformation occurs when the particles kinetic energy (to cause local stresses) is higher than the yield strength of the test material. Cutting occurs when the particles have sufficient energy to shear the local surface.

The morphology of the wear scars shows that the impact angles of solid particles are very small. The solid particles scratch the specimen surface, resulting in a larger scar elongated in the direction of particle motion. Because erosion increases with the increase of sand concentration, more wear scars are found with the increase of sand concentration under the same flow rate. Compare the morphology of Figure 4-25 (a) and (b).

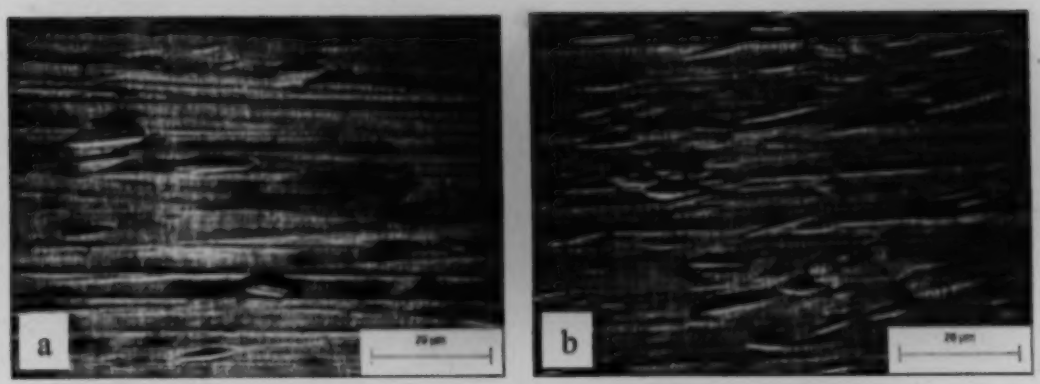

Figure 4-25 Surface morphology in flowing slurry under cathodic protection for 30 minutes at 6000 RPM
(a) 10 wt% sand (b) 20 wt% sand

4.6.2.3 Surface morphology produced by slurry erosion

Erosion-corrosion tests were conducted for 30 minutes in slurry with 20 wt% sand at 6000 RPM under an open circuit condition. Not only lots of wear scars and uniform corrosion were found, but also many erosion-corrosion pits on the surface after the erosion-corrosion test. The plastic deformation effect caused by solid particle impact leads to the presence of dislocations, defects and stress. This would accelerate the activity of the impact site, leading to greatly accelerated corrosion.

Erosion-corrosion pits are shown in Figure 4-26 (a). The geometry of the pits is very different from the wear scars. The pits appear more irregular and have a bigger dimensional size than the wear scars shown in Figure 4-26 (b). Also, the corrosion pits are much deeper than the wear scars, which are shown in Figure 4-27 (a) after polishing the surface. The wear scars were easily removed, while the corrosion pits became more obvious after polishing. The surface was also etched to find the location of the pits. We still find that most pits occur on the grain boundary between ferrite and pearlite or in pearlite, as shown in Figure 4-27 (b). A more detail of one of the pits is shown in Figure 4-28 (taken by SEM).

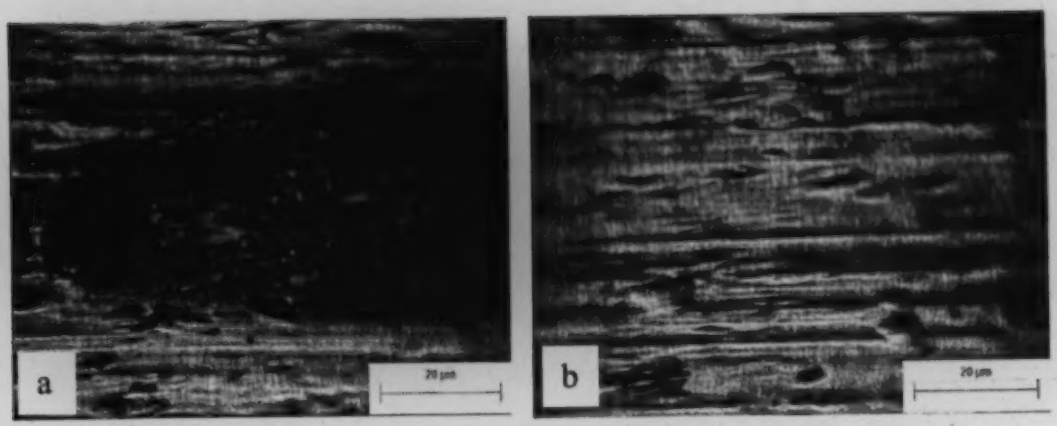

Figure 4-26 Surface morphology in flowing slurry with 20 wt% sand under open circuit for 30 minutes at 6000 RPM
(a) erosion-corrosion pit (b) wear scar

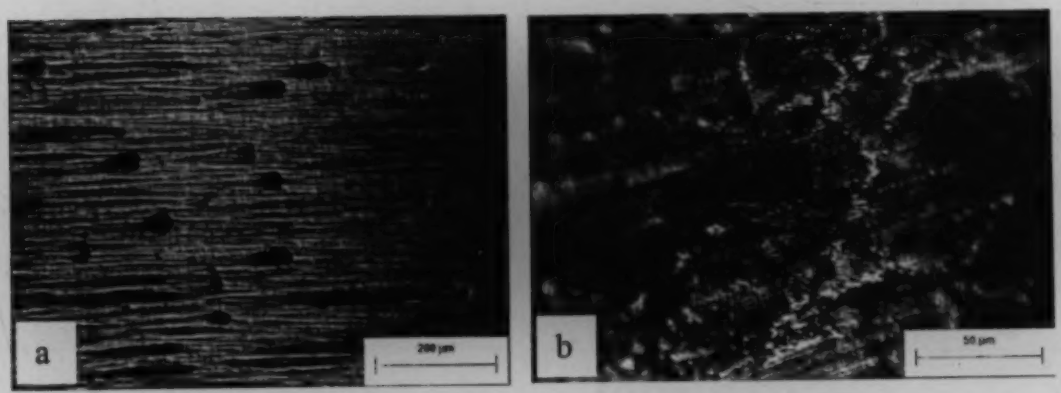

Figure 4-27 Surface morphology in flowing slurry with 20 wt% sand under open circuit for 30 minutes at 6000 RPM
(a) after polishing (b) after polishing and etching

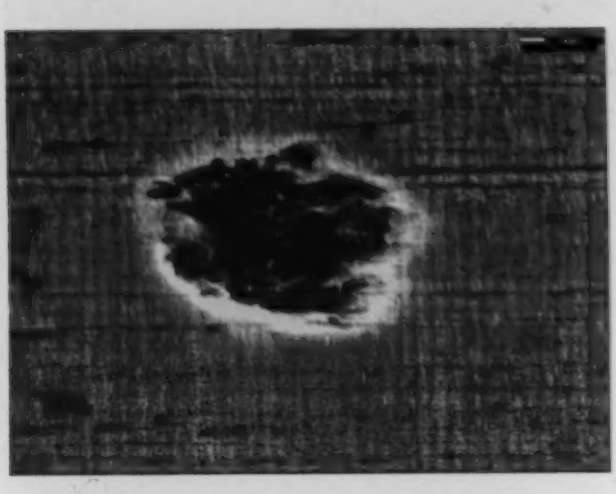

Figure 4-28 The SEM micrograph showing deep pit in flowing slurry with 20 wt% sand under open circuit for 30 minutes at 6000 RPM

Figure 4-29 is the surface morphology after erosion-corrosion in slurry with 20 wt % sand for 25 hours under an open circuit condition. Even more pits (with big dimensions) were found. The pits are linked up in the direction of flow. The dimension of pits is probably bigger than that of the pearlite grain size. As said before, preferential corrosion (pit) at grain boundaries will result in grain loosening. Therefore, mechanical erosion is enhanced.

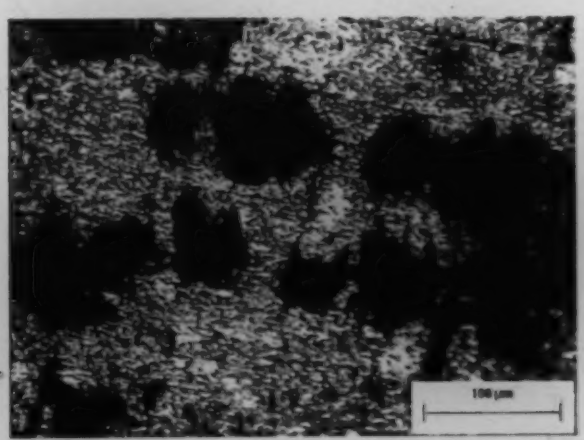

Figure 4-29 Surface morphology after erosion-corrosion for 25 hours in slurry with 20 wt% sand under open circuit at 6000 RPM

Figure 4-30 is the surface morphology in slurry with 20 wt% sand under 2.5E-4 A/cm^2 anodic polarization for 30 minutes at 6000 RPM. We can see that the number of pits increases with the increase of erosion and corrosion by comparing with that in static tap water (Figure 4-21), flowing water (Figure 4-22) and flowing slurry (Figure 4-27 (a)) under an open circuit condition. They were all taken at the same magnification. This means that the pitting effect was enhanced by increasing the corrosion activity.

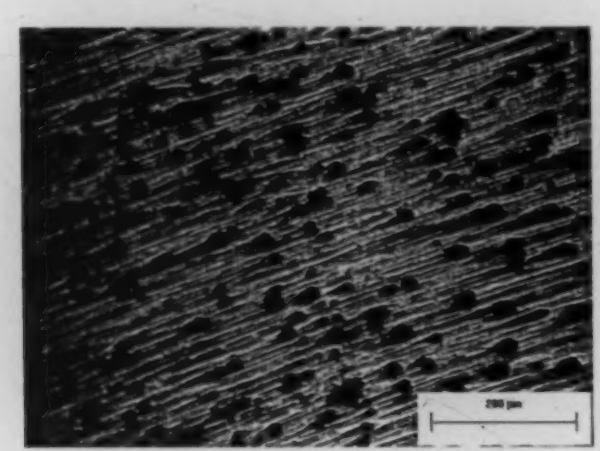

Figure 4-30 Corrosion pits in slurry with 20 wt% sand, 2.5E-4A/cm^2 anodic polarization for 30 minutes at 6000 RPM

4.6.2.4 Comparison of wear scars and pits

(1) Wear scars

According to hardness tests, hardness decreases under an anodic polarization because of the chemo-mechanical effect. From the weight loss test under cathodic protection for materials with different hardness, the results show that the pure erosion rate increases with a decrease in hardness. If the hardness decreases greatly under anodic polarization, it is expected that the wear scar under anodic polarization should be bigger than that under cathodic protection, because of the chemo-mechanical effect.

The SEM results for wear scars under anodic polarization are compared with that under cathodic protection, shown in Figure 4-31. The time duration was only 10 minutes, so that the surface was not obviously corroded under anodic polarization. The size of the wear scar is statistically analyzed in Figure 4-32.

From the observations and analyses of the surface morphology under different conditions, we can see that there is no obvious change of wear scars in slurry whether it is in cathodic protection or anodic polarization. The wear scars under anodic polarization are a little bit shallower and smaller than that under cathodic protection, illustrated by the difference in the depth of scars in Figure 4-31 and Figure 4-32, respectively. This is because anodic dissolution occurred during the forming process of wear scars. Anodic dissolution would reduce the wear scar sizes measured after the test finished. This shows that hardness degradation because of the chemo-mechanical effect is not the main reason for the synergy, which is consistent with the hardness test results.

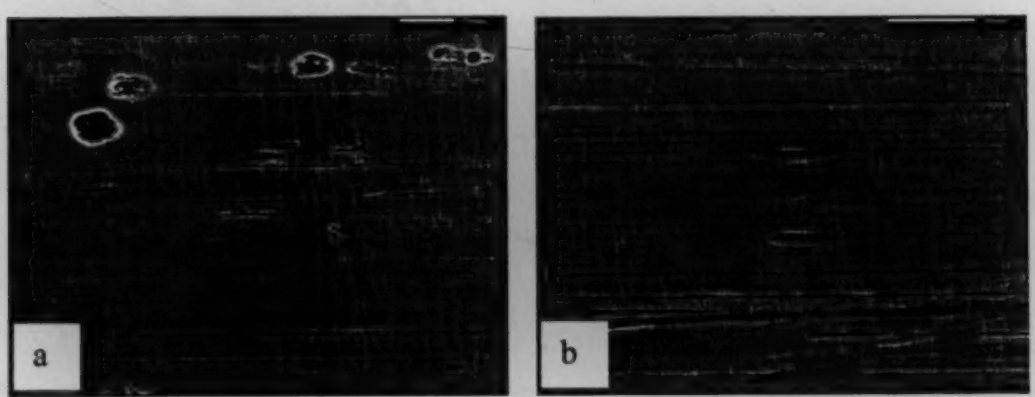

Figure 4-31 Comparison of the morphology of wear scars in slurry with 20 wt% sand for 10 minutes at 6000 RPM

(a) 2.5E-4 A/cm2 anodic polarization (b) cathodic protection

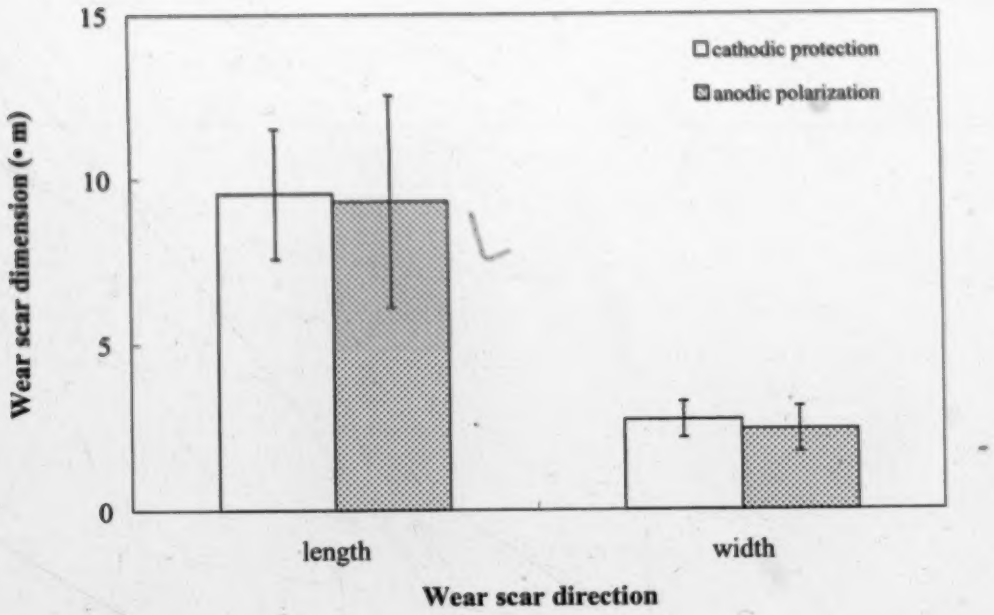

Figure 4-32 Comparison of the dimensions of wear scars in slurry with 20 wt% sand for 10 minutes at 6000 RPM under cathodic protection and 2.5E-4 A/cm^2 anodic polarization

(2) Pits

The pit number and area fraction of pits under different conditions were statistically analyzed, shown in Figure 4-33 and Figure 4-34. Surface morphology analyses found that there is a lower pit number under static and flowing tap water. Under cathodic protection, there is no pit at all. However, there is a much higher pit number and area fraction in slurry because of the introduction of solid particles. The development of pits must be caused by the synergistic effect between erosion and corrosion. Therefore, the main reason for synergy is the non-uniform corrosion caused by pits.

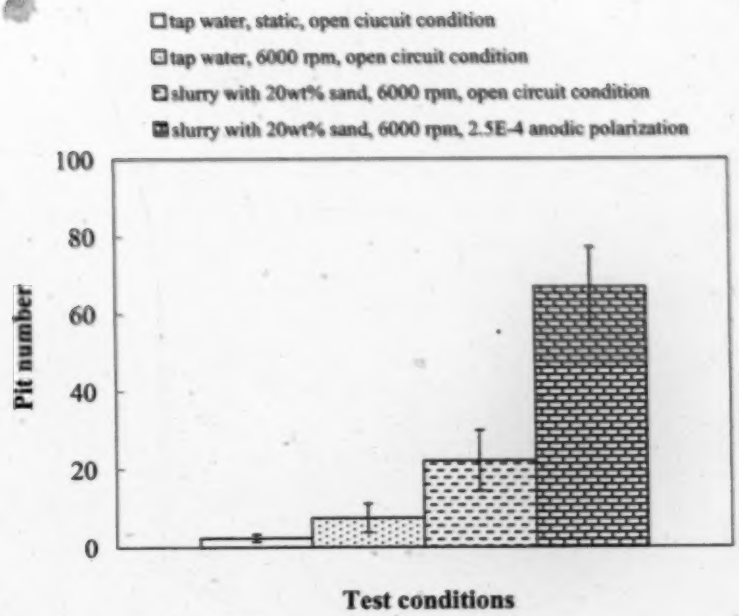

Figure 4-33 Comparison of pit number in different test conditions for 30 minutes

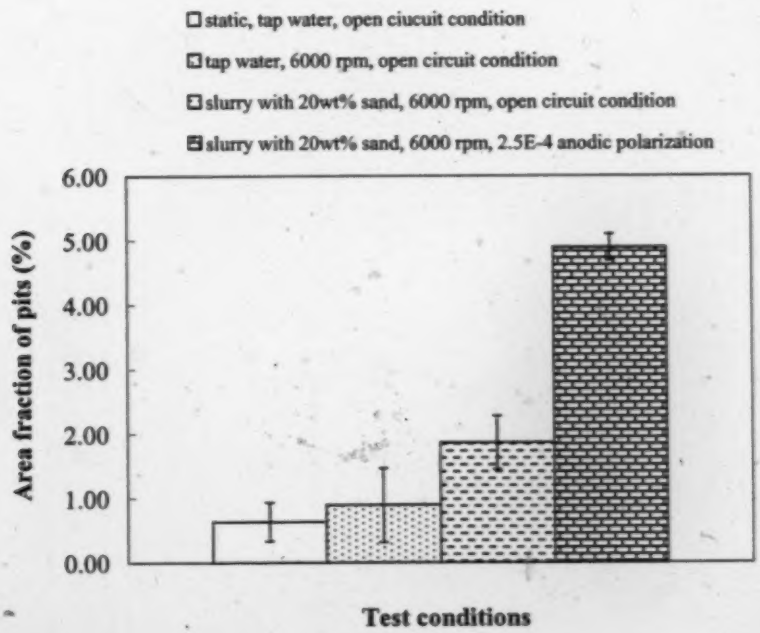

Figure 4-34 Area fraction of pits in different test conditions for 30 minutes

4.6.3 Mechanism of the synergy

From the above analyses, erosion-corrosion is a mutual process. Erosion can enhance corrosion and vice versa, leading to the important synergistic effect.

For the effect of erosion on corrosion, there are several aspects.

(1) The repeated impact of hard silica sand particles on a specimen surface can break down the oxide film, remove corrosion product and expose fresh metal; therefore corrosion is enhanced.[43,44]

(2) The erosion will promote anodic dissolution and oxygen diffusion in the boundary layer of the electrolyte, resulting in an acceleration of corrosion.

(3) Plastic deformation is induced because of the impact of solid particles, leading to the presence of dislocations, defects and stress. This would accelerate the activity of the impact site, leading to greatly accelerated corrosion.

The corrosive attack on the specimen surface can also aid the erosion process for the following reasons:

(1) By the chemo-mechanical effect, the underlying base metal is removed more easily by mechanical forces, resulting from the erosion process.

(2) The micro-galvanic effect between ferrite and cementite exists because of the two-phased microstructure of A1045 carbon steel. Pits occur on the surface of the specimen because of the micro-galvanic effect. Cementite is dissolved preferentially. Then the material loses its erosion resistance because of low hardness of the remaining ferrite matrix. The development of pits is further enhanced by the effect of solid particles. From the surface morphology analysis, this is the most important factor introducing the synergy effect.

Chapter 5 Conclusions and future work

5.1 Conclusions

From the above results and analyses, the following conclusions are obtained:

1. The micro-hardness of steel decreases with the increase of anodic current density on the surface because of a chemo-mechanical effect. The normalized hardness drop $\Delta Hv / Hv_0$ is a linear function of the logarithm of the anodic current density and the correlation of $\Delta Hv / Hv_0$ vs. anodic current density is almost independent of the polarization behavior of materials.

2. The combination of electrochemical, weight loss and visual/microscopic/SEM investigations has quantified the three basic features of materials degradation—pure erosion, pure corrosion and synergy in erosion-corrosion conditions. The synergy between erosion and corrosion increases with the increase of flow rate and sand concentration. In some conditions, the synergistic effect can account for one third of the total weight loss.

3. The rate of material loss produced by the synergy increases with increasing anodic current density while the pure mechanical erosion rate increases with decreasing hardness, indicating that the hardness degradation due to chemo-mechanical effect is a synergistic mechanism in slurry-erosion processes.

4. Based on the surface morphology analysis, the corrosion of A1045 carbon steel in flowing slurry is a non-uniform process. Pits form on the surface of the specimen because of the micro-galvanic effect between ferrite and cementite. Cementite tends to be dissolved preferentially. Then the material loses its erosion resistance because of low hardness of the remaining ferrite matrix. The impingement of sand particles and anodic polarization can promote the formation of pits, indicating pits may contribute to the synergism in the slurry-erosion process.

5.2 Future work

There are several things that need to be further investigated.

First, the mechanism of pitting development in the erosion-corrosion process needs to be studied. Since electrochemical noise measurement is widely used in the study of pitting corrosion, it can be used in this study to clarify the synergy mechanism.

Second, the contribution of pitting to the synergy also needs to be quantified.

Third, more investigations should also be conducted to understand the role of the chemo-mechanical effect in other systems in the erosion-corrosion processes.

Literature Cited

1 H. M. Clark and R. J. Llewellyn, "Assessment of the erosion resistance of steels used for slurry handling and transport in mineral processing applications", **Wear**, Vol. 250 (2001), p. 32-44.

2 A. J. Buchan and A. J. S. Speearing, "The effect of corrosion on the wear rate of steel pipelines conveying backfill slurry", **Journal of the South African Institute of Mining and Metallurgy**, (1994), p. 37-45.

3 A. Neville, T. Hodgkiess, J.T. Dallas, "A study of the erosion-corrosion behavior of engineering steels for marine pumping applications", **Wear**, Vol. 186-187 (1995) p. 497-507.

4 A. Neville and T. Hodgkiess, "Study of effect of liquid corrosivity in liquid-solid impingement on cast iron and austenitic stainless steel", **British Corrosion Journal**, Vol. 32(3) (1997), p. 197-205.

5 S. Zhou, M.M. Stack, and R.C. Newman, "Electrochemical studies of anodic dissolution of mild steel in a carbon-bicarbonate buffer under erosion-corrosion conditions", **Corrosion Science**, Vol. 38 (7) (1996), p. 1071-1084.

6 G.R. Hoey and J.S. Bednar, "Erosion-corrosion of selected metals in coal washing plant environment", **Materials Performance**, Vol. 22(4) (1983), p. 9-14.

7 W.H.W. Husband, Editor, Saskatchewan Research Council, **Slurry Pipeline Manual Design and Construction**, 1986.

8 ASTM Standard G-40 "Standard Terminology Relating to Erosion and Wear", Philadelphia, PA

9 Ian M. Hutchings, **Erosion of Materials by Liquid Flow**, MTI publication No 25, 1986.

10 R.J.K. Wood, J.A. Wharton, A.J. Speyer and K.S. Tan, "Investigation of erosion-corrosion processes using electrochemical noise measurements", **Tribology International,** Vol. 35 (2002), p. 631-641.

11 E. Heitz, "Chemo-mechanical effects of flow on corrosion", **Corrosion**, Vol. 47(2) (1991), P. 135-145.

12 Finnie, I., Wolak, J. and Kabil, Y., "Erosion of metals by solid particles", **Journal of Materials**, Vol. 2 (1967), p. 682-700.

13 Bellman, R., Jr., and Levy, A. V., "Erosion mechanism in ductile metals", **Wear**, Vol. 70(1) (1981), p. 1-28.

14 Alan Levy, **Solid Particle Erosion and Erosion-corrosion of Materials**, Materials Park, OH: ASM International, 1995, p. 11.

15 I. Finnie, "Some observations on the erosion of ductile metals", **Wear**, Vol. 19 (1972), p. 81-90.

16 I. Finnie, "Some reflections on the past and future of erosion", **Wear**, Vol. 186-187 (1995), p. 1-10.

17 J.G.A, Bitter, "A study of erosion phenomena Part I", **Wear**, Vol. 6 (1963), p. 5-21.

18 J.G.A. Bitter, "A study of erosion phenomena Part II", **Wear**, Vol. 6 (1963), p. 169-190.

19 I. M. Hutchings, "A model for the erosion of metals by spherical particles at normal incidence", **Wear**, Vol. 70 (1981), p. 269-281.

20 G. Sundararajan and P. G. Shewmon, "A new model for the erosion of metals at normal incidence", **Wear**, Vol. 84 (1983), p. 237-285.

21 G. Sundararajan, "A compressive model for the solid particle erosion of ductile materials", **Wear**, Vol. 149 (1991), p. 111-127.

22 J. M. Link, "Pipe wear in hydraulic transport of solids", **Mining Congress Journal**, Vol. 58(7) (1972), P. 38-43.

23 Finnie, I., "The Mechanism of Erosion in Ductile Materials", **Proc. of the Third US National Congress of Applied Mechanics**, Hagthormthwaite, R. M., Ed., ASME, New York, (1958), p. 78-82.

24 B. W. Madsen, "A study of parameters using a new constant-wear-rate slurry test", **Wear of Materials**, ASME, (1985), p. 345-354.

25 S. Weber, R. Liebe, E. Heitz "Erosion corrosion and erosion of various materials in high-velocity flows containing particles," in **Flow-induced Corrosion: Fundamental Studies and Industry Experience**, K. J. Kennelly, R. H. Hausler, D. C. Silverman. Eds. Houston, TX: NACE, 1991.

26 G. F. Truscott, "A literature survey on abrasive wear in hydraulic machinery", **Wear**, Vol. 20 (1972), P. 29-50.

27 Liebhard M., and Levy, A. V., "The effect of erodent particle characteristics on the erosion of metals", **Wear**, Vol. 151(2) (1991), p. 381-390.

28 ASM Metals Handbook, Vol.10, **Liquid-erosion Failure**, F.G. Hammitt and F.J. Heymann, ASM, Materials Park, OH, 1975.

29 S. Endo and M. Nagae, "Comparison of experimentally measured and theoretically predicted erosion rates of steels in slurries of low velocity", **ISIJ International**, Vol. 36(1) (1996), p. 87-94.

30 Samuel A. Brandford, **Corrosion Control**, second edition, Edmonton: CASTI Publishing Inc, c2002.

31 G. Kreysa, **Principles of Electrochemical Engineering**, New York, VCH Publishers, 1986.

32 U. Lotz and E. Heitz, **Werkstoffe U. Korrosion**, Vol. 34 (1983), p. 454.

33 **Corrosion: Understanding the Basics**, Materials Park, Ohio: ASM International, 2000.

34 G.J. Bignold, K. Garbett, R. Garnsey and I.S. Woolsey, **Proc. Conf. on Water Chemistry**, BNES, 1980, Paper I.

35 Y.G. Zheng, Z.M. Yao, X.Y. Wei and W. Ke, "The synergistic effect between erosion and corrosion in acidic slurry medium", **Wear**, Vol. 186-187 (1995), p. 555-561.

36 R.T. Knapp, J.W. Daily and F.G. Hammitt, **Cavitation**, McGraw-Hill, New York, 1970.

37 H.S. Campbell and V.E. Carter, "A laboratory investigation of high-tensile brass propeller wastage", **Journal of the Institute of Metals**, Vol. 90 (1961-1962), p. 362-367.

38 H. Hocke and H. N.Wilkinson, "Testing abrasion resistance of slurry pipeline materials", **Tribology International**, Vol. 11(1978), p. 289-294.

39 W.A. Stauffer, "Wear of metals by sand erosion", **Metal Progress**, (1956), p. 102-107.

40 B. Poulson, "Complexities in predicting erosion corrosion", **Wear**, Vol. 233-235 (1999), p. 497-504.

41 M. Reyes, and A. Neville, "Mechanism of erosion-corrosion on a Cobalt–based alloy and stainless-steel UNS S17400 in aggressive slurries", **J. Materials Engineering and Performance**, Vol. 10(6) (2001), p. 723-730.

42 X. Jiang, S. Li, D. Tao and J. Yang, "Accelerative effect of wear on corrosion of high-alloy stainless steel", **Corrosion**, Vol. 49(10) (1993), p. 836-841.

43 J. Postlethwaite, M. W. Hawrylak, "Effect of slurry abrasion on the anodic dissolution of iron in water", **Corrosion**, Vol. 31(7) (1975), p. 237-240.

44 J. Postlethwaite, M. H. Dobbin and K. Bergevin, "The role of oxygen mass transfer in the erosion-corrosion of slurry pipelines", **Corrosion**, Vol. 42(9) (1986), p. 514-521.

45 X.Z. Zhao, N. Cui, J.L. Luo, S. Chiovelli, "Effect of erosion on corrosion of type 430 and 316 stainless steels in aqueous environment", **British Corrosion Journal**, Vol. 37(1) (2002), p. 63-68.

46 J. Postlethwaite, "Effect of chromate inhibitor on the mechanical and electrochemical components of erosion-corrosion in aqueous slurries of sand", **Corrosion**, Vol. 37(1) (1981), p. 1-5.

47 R. J. K. Wood, "The synergistic effect of erosion and corrosion: trends in published results", **Wear**, Vol. 140 (1990), p. 387-394.

48 R. Perez, and J.J. Moore, "The influence of grinding ball composition and wet grinding conditions on metal wear", **Wear of Materials,** (1983), p. 67.

49 R. J. Neol and A. Ball, "On the synergistic effects of abrasion and corrosion during wear", **Wear of Materials,** (1983), p. 148-152.

50 J. Heidemeyer, "Influence of the plastic deformation of metals during mixed friction on their chemical reaction rate", **Wear**, Vol. 66 (1981), p. 379-387.

51 K.Y. Kim, S. Bhattacharyya and V.Agarwala, "An electrochemical polarization technique for evaluation of wear-corrosion in moving components under stress", **Wear of Materials**, (1981), ASME, p. 772-778.

52 X.Y. Wei, Y.G. Zheng, Y.S. Zhang, Z.M. Yao, Y.D. Zhang, S.P. Zhang, W. Ke, "Effect of microstructure and element distribution on erosion-corrosion behaviour of an iron base cast alloy", **Acta Metallurgica Sinica** (Chinese Edition), Vol. 30(2) (1994), A91-A96.

53 A. Neville and X. Hu, "Mechanical and electrochemical interactions during liquid–solid impingement on high-alloy stainless steels", **Wear**, Vol. 251 (2001), p.1284-1294.

54 S. Zhou, M.M. Stack, and R.C. Newman, "Characterization of synergistic effects between erosion and corrosion in an aqueous environment using electrochemical techniques", **Corrosion Science**, Vol. 52 (1996), p. 934-946.

55 R.J.K. Wood, S.P. Hutton, "The synergistic effect of erosion and corrosion: trends in published results", **Wear**, Vol. 140 (1990), p. 387-394.

56 Y. Li, I.M. Hutching, G.T. Burstein, "The influence of corrosion on the erosion of aluminum by aqueous silica slurries", **Wear**, Vol. 186-187 (1995), p. 515-522.

57 B. W. Madsen, "Measurement of erosion-corrosion synergism with a slurry wear test apparatus", **Wear**, Vol. 123 (1988), p. 127-142.

58 Z. Yue, P. Zhou, and J. Shi, "Some factors influencing corrosion-erosion performance of materials", **Wear of Materials**, ASME, New York, (1987), p. 763-771.

59 E. M. Gutman, **Mechanochemistry of Metals and Corrosion Protection**, Metallurgiya, Moscow, 2nd Ed., 1981.

60 E. M. Gutman, **Mechanochemistry of Solid Surfaces**, World Scientific, 1994.

61 J. Larsen-Basse and H. Liang, "Probable role of abrasion in chemo-mechanical polishing of tungsten", **Wear**, Vol. 233-235 (1999), p. 647-654.

62 A. Neville, H. Xu and M. Reyes, "Corrosion and erosion-corrosion behavior of a Co-based alloy and a Ni-containing austenitic cast iron", **Corrosion 2000**, NACE International, Houston, p. 00628.1-00628.12.

63 U. Lotz and T. Sydberger, "CO_2 corrosion of carbon steel and 13Cr steel in particle-laden fluid", **Corrosion Science**, Vol. 44(11) (1988), p. 800-809.

64 D. He, X. Jiang, S. Li and H. Guan, "Erosion and erosion-corrosion behaviors of several stainless steels in dual-phase fluid", **Corrosion**, Vol. 58(3) (2002), p. 276-282.

65 T. Hodgkiess, A. Neville and S. Shrestha, "Electrochemical and mechanical interactions during erosion-corrosion of a high-velocity oxy-fuel coating and a stainless steel", **Wear**, Vol. 233-235 (1999), p. 623-634.

66 H.M. Shalaby, S. Attari, W.T. Riad and V.K. Gouda "Erosion-corrosion behavior of some cast alloys in seawater", **Corrosion**, Vol. 48(3) (1992), p. 206-217.

67 Z. Xia, K.C. Chou and Z. Szklarska-Smialowska, "Pitting corrosion of carbon steel in CO_2-containing NaCl brine", **J. Science & Engineering Corrosion**, Vol. 85(8) (1989), p. 636-642.

68 http://www.corrosion-doctors.org/Forms/erosion.htm.

69 G. T.Burstein and K. Sasaki, "The birth of corrosion pits as stimulated by slurry erosion", **Corrosion Science**, Vol. 42 (2000), p. 841-860.

70 Uchida. T, "Influence of suspended solids on pitting corrosion of carbon steel in cooling water", **J. Soc. Mater. Sci.**, Japan, Vol. 42(479) (1993), p. 912-916.

71 http://www.epcor.ca/pages/water/waterquality/daily/wqdaily.htm.

72 ASTM G3-89, "Standard Practice for Conventions Applicable to Electrochemical Measurements in Corrosion Testing".

73 NACE Standard RP-01-69, "Recommended Practice, Control of External Corrosion on Underground or Submerged Metallic Piping Systems", Revision, NACE, Houston, 1983.

74 Gummow, R.A., "Cathodic protection criteria: a critical review of NACE standard RP-01-69", **Materials Performance**, Vol. 25(9) (1986), p. 9-16.

75 ASTM G1-90, "Standard Practice for Preparing, Cleaning and Evaluating Corrosion Test Specimens".

76 A. H. Cottrell, **Theory of Crystal Dislocations**, New York, Gordon and Breach (1964), Science Publishers.

77 Z.Q. Cui, **Metallurgy and Heat Treatment**, Mechanical industry publisher, (1988).

78 J.C.M. Li, "Some dislocation mechanisms in deformation, recovery and recrystallization of metals", **Journal of the Australian Institute of Metals**, Vol. 8(2) (1963), p. 206-221.

79 William D. Callister, JR., **Materials Science and Engineering An I ntroduction**, 4th edition, NewYork: John Wiley & Sons, c1997, p.160.

80 C.H. Wu, X.H. Mao, F.X. Gan, "Study of the erosion-corrosion electrochemical behavior of carbon steel in multiphase flowing fresh water", **Materials Protection**, Vol. 34(11) (2001), p. 3-5.

81 S. Aso, S. Goto, Y. Komatsu, W. Liu and C. Liu, "Slurry erosion of Fe-15 mass%/25 mass% Cr–C–B eutectic alloys", **Wear**, Vol. 233-235 (1999), p. 160-167.

82 H.J. Cleary and N.D. Greene, "Electrochemical properties of Fe and steel", **Corrosion Science**, Vol. 9(1) (1969), p. 3-13.

83 H. J. Cleary and N. D. Greene, "Corrosion properties of iron and steel", **Corrosion Science**, Vol. 7(12) (1967), p. 821-831.

84 S. Al-Hassan, B. Mishra, D.L. Olson, and M.M. Salama, "Effect of microstructure on corrosion of steels in aqueous solutions containing carbon dioxide", **Corrosion**, Vol. 54(6) (1998), p. 480-491.